RESEARCH ARTICLE

The TAF10-containing TFIID and SAGA transcriptional complexes are dispensable for early somitogenesis in the mouse embryo

Paul Bardot[1,2,3,4,§], Stéphane D. Vincent[1,2,3,4,§,**], Marjorie Fournier[1,2,3,4,*,¶], Alexis Hubaud[1,2,3,4,‡,¶], Mathilde Joint[1,2,3,4], László Tora[1,2,3,4] and Olivier Pourquié[1,2,3,4,‡]

ABSTRACT

During development, tightly regulated gene expression programs control cell fate and patterning. A key regulatory step in eukaryotic transcription is the assembly of the pre-initiation complex (PIC) at promoters. PIC assembly has mainly been studied *in vitro*, and little is known about its composition during development. *In vitro* data suggest that TFIID is the general transcription factor that nucleates PIC formation at promoters. Here we show that TAF10, a subunit of TFIID and of the transcriptional co-activator SAGA, is required for the assembly of these complexes in the mouse embryo. We performed *Taf10* conditional deletions during mesoderm development and show that *Taf10* loss in the presomitic mesoderm (PSM) does not prevent cyclic gene transcription or PSM segmental patterning, whereas lateral plate differentiation is profoundly altered. During this period, global mRNA levels are unchanged in the PSM, with only a minor subset of genes dysregulated. Together, our data strongly suggest that the TAF10-containing canonical TFIID and SAGA complexes are dispensable for early paraxial mesoderm development, arguing against the generic role in transcription proposed for these fully assembled holo-complexes.

KEY WORDS: RNA polymerase II, TATA binding protein, Presomitic mesoderm, Paraxial mesoderm, Conditional knockout, Proteomic, Mouse

INTRODUCTION

In mouse, the posterior part of the paraxial mesoderm, called presomitic mesoderm (PSM), generates a pair of somites every 2 h and plays crucial roles during vertebrate elongation (Pourquié, 2011). This rhythmic process is under the control of a clock that is characterized by periodic waves of transcription of cyclic genes sweeping from the posterior to the anterior PSM (Hubaud and Pourquié, 2014). In the anterior PSM, the clock signal is converted into a stripe of expression of specific segmentation genes that

[1]Institut de Génétique et de Biologie Moléculaire et Cellulaire, Illkirch 67400, France. [2]Centre National de la Recherche Scientifique, UMR7104, Illkirch 67400, France. [3]Institut National de la Santé et de la Recherche Médicale, U964, Illkirch 67400, France. [4]Université de Strasbourg, Illkirch 67400, France.
*Present address: Sir William Dunn School of Pathology, University of Oxford, Oxford OX1 3RE, UK. ‡Present address: Brigham and Woman's Hospital, Harvard Medical School, Boston, MA 02115, USA.
§These authors contributed equally to this work
¶These authors contributed equally to this work

**Author for correspondence (vincent@igbmc.fr)

S.D.V., 0000-0003-1638-9615; M.F., 0000-0002-5202-8262; A.H., 0000-0003-1249-4282; M.J., 0000-0002-6497-4328; L.T., 0000-0001-7398-2250

defines the future somite. This periodic transcription initiation associated with the segmentation clock oscillations in the PSM offers a unique paradigm with which to study transcriptional regulation in development.

During embryogenesis, gene expression is regulated by a combination of extracellular signals triggering intracellular pathways, which converge towards the binding of transcription factors to enhancers and promoters. These interactions lead to the assembly of the transcriptional machinery. In non-plant eukaryotes, three RNA polymerases are able to transcribe the genome, among which RNA polymerase II (Pol II) is responsible for the production of mRNA and some of the non-coding RNAs (Levine et al., 2014 and references therein).

Transcription initiation requires the assembly of the pre-initiation complex (PIC) that allows the correct positioning of Pol II on the promoter and consequent RNA synthesis (Sainsbury et al., 2015). TFIID is the first element of the PIC recruited to active promoters. In its canonical form in higher eukaryotes it is composed of TATA binding protein (TBP) and 13 TBP-associated factors (TAFs) and is involved in the correct positioning of Pol II on the transcription start site. Whereas TBP is also part of Pol I and Pol III transcription complexes, the TFIID-TAFs are specific for Pol II transcription machinery. Among the metazoan TAFs, TAF9, TAF10 and TAF12 are also shared by Spt-Ada-Gcn5-acetyl transferase (SAGA) complex, which is a transcriptional co-activator conserved from yeast to human (Spedale et al., 2012). SAGA exhibits histone acetyltransferase activity at promoters and also deubiquitylates histone H2Bub1 in gene bodies (Bonnet et al., 2014; Wang and Dent, 2014; Weake et al., 2011).

Several structural TAFs, including TAF10, share a histone fold domain (HFD) which is involved in their dimerization with specific partners: TAF10 heterodimerizes with TAF3 or TAF8 within TFIID and with SUPT7L/ST65G within SAGA (Leurent et al., 2002; Soutoglou et al., 2005). Nuclear import of TAF10 is absolutely dependent on heterodimerization with its partners since TAF10 does not have a nuclear localization signal (NLS) (Soutoglou et al., 2005).

TAF10 does not exhibit any enzymatic activity but serves as an interface allowing interaction with other TAFs (Bieniossek et al., 2013; Trowitzsch et al., 2015) or transcription factors, such as the human estrogen receptor α (Jacq et al., 1994) or mouse GATA1 (Papadopoulos et al., 2015). In HeLa cells, only 50% of the TFIID complexes contain TAF10 (Jacq et al., 1994). TFIID complexes lacking TAF10 have also been observed in mouse F9 cells although at much lower level (Mohan et al., 2003), but their functionality is unknown. The structure of TFIID in the absence of TAF10 is unclear. Only partial TFIID subcomplexes, not associated with TBP, were detected in undifferentiated and retinoic acid (RA)-differentiated *Taf10* mutant F9 cells (Mohan et al., 2003), while lack

DEVELOPMENT

of TFIID was observed in *Taf10* mutant liver cells (Tatarakis et al., 2008). SAGA was not investigated in these experiments (Mohan et al., 2003; Tatarakis et al., 2008). Altogether, these data support the idea that TFIID composition can vary, as also suggested by the existence of TAF paralogs and/or tissue-specific TAFs (Goodrich and Tjian, 2010; Müller et al., 2010).

The diversity in TFIID composition may have functional consequences. Whereas TAF10 is crucial for survival and proliferation of F9 cells, it is dispensable for their differentiation into primitive endoderm (Metzger et al., 1999). *Taf10* mutation in mouse leads to embryonic lethality shortly after implantation (Mohan et al., 2003). Interestingly, whereas inner cell mass cells die by apoptosis, trophoectodermal cells survive, although Pol II transcription is greatly reduced (Mohan et al., 2003). *Taf10* conditional deletion in skin or liver has shown that TAF10 is required for transcription in the embryo, but not in the adult (Indra et al., 2005; Tatarakis et al., 2008). Altogether, these data indicate that TAF10 requirement depends on the cellular and developmental context.

In this study, we aimed to closely analyze TAF10 requirement and its role in transcription during mouse development, and to examine the composition of TFIID and SAGA in the absence of TAF10 in embryonic tissues *in vivo*. We performed immunoprecipitations coupled to mass spectrometry analyses on embryonic lysates. We show that, in the mouse embryo, absence of TAF10 severely impairs TFIID and SAGA assembly. In order to gain insight into the functional importance of TAF10 during development, we focused on paraxial mesoderm dynamic differentiation by carrying out a *Taf10* conditional deletion in the mesoderm using the *T-Cre* line (Perantoni, 2005). Although loss of *Taf10* eventually led to growth arrest and cell death at ~E10.5, we identified a time window during which the dynamic transcription of cyclic genes is still maintained in the absence of detectable TAF10 protein. Microarray analysis of mutant PSM revealed that Pol II transcription is not globally affected in this context, although the expression of some genes, such as those encoding cell cycle inhibitors, is upregulated.

RESULTS

TAF10 is ubiquitously expressed in the nucleus of embryonic cells at E9.5

Taf10 is ubiquitously expressed in the mouse embryo at E3.5, E5.5 and E7.5 but with more heterogeneity at E12.5 (Mohan et al., 2003). Whole-mount *in situ* hybridization (WISH) analyses suggest that *Taf10* is also ubiquitously expressed at E8.5 and E9.5 (Fig. S1A,B). TAF10 protein is ubiquitously expressed in the posterior part of the embryo (Fig. S1C, Fig. S2) and no heterogeneity was observed between E9.5 and E10.5. Competition with the peptide used to raise the anti-TAF10 antibody (Mohan et al., 2003) confirms that TAF10 localization is specific, since the TAF10 signal, but not the myogenin signal, is lost under these conditions (Fig. S1D,H). Altogether, these results indicate that TAF10 protein is ubiquitously expressed in nuclei between E8.5 and E10.5.
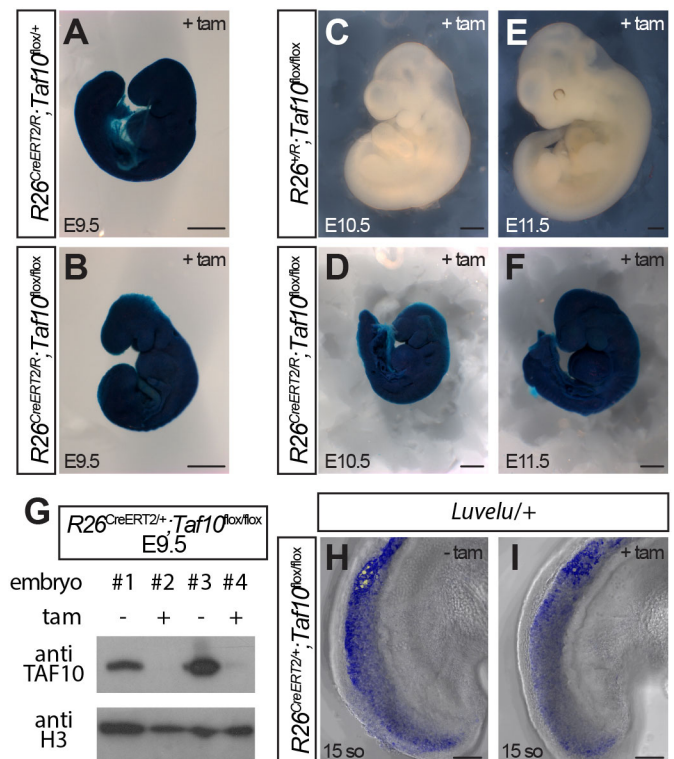
Induced ubiquitous deletion of *Taf10* leads to growth arrest at E10, but does not impair transcription at E9.5

In order to analyze the effects of TAF10 absence on development, we performed a tamoxifen-inducible ubiquitous deletion of *Taf10* using the *R26*[CreERT2] line (Ventura et al., 2007). This strategy deletes exon 2 of *Taf10*, which encodes part of the HFD (Mohan et al., 2003), and because exon 3 is now out of frame the deletion is expected to produce a truncated protein of 92 amino acids

without an HFD (Fig. S3D). Since the HFD is required for heterodimerization and integration of TAF10 into TFIID and SAGA (Leurent et al., 2002; Soutoglou et al., 2005), this potential truncated protein is not supposed to integrate into mature SAGA or TFIID complexes. Tamoxifen was injected intraperitoneally at E7.5 and Cre recombination was followed by the activity of the Cre reporter allele *R26*[R] (Soriano, 1999). Complete Cre recombination is observed at E9.5 (Fig. 1A,B). The development of *R26*[CreERT2/+]; *Taf10*[flox/flox] (*R26Cre;Taf10*) mutant embryos was arrested at E9.5, as embryos do not further develop when recovered at E10.5 and E11.5 (Fig. 1D,F). The normal development of *R26*[R/+];*Taf10*[flox/flox] littermate embryos (Fig. 1C,E) confirmed that tamoxifen injection at E7.5 does not induce secondary defects.

Efficient TAF10 depletion at E9.5 after tamoxifen injection at E7.5 was assessed by western blot (Fig. 1G). At E8.5 TAF10 was still present, albeit at lower levels (Fig. S3E). This observation is in agreement with a previous study in which TAF10 protein was still detected one day after induction of its depletion (Metzger et al., 1999). Since our goal is to assess TFIID and SAGA composition in the absence of TAF10, we performed our analyses at E9.5.

In order to assess transcription initiation *in vivo*, we used the *Luvelu* reporter line (Aulehla et al., 2008) that allows visualization of the dynamic waves of *Lfng* transcription occurring every 2 h in the posterior PSM. This line contains the promoter and 3′-UTR destabilizing sequences of the cyclic gene *Lfng* (Cole et al., 2002; Morales et al., 2002), coupled to the coding sequences of a

Fig. 1. Efficient ubiquitous deletion of *Taf10* in E9.5 *R26Cre;Taf10* mutant mouse embryos. (A-F) Whole-mount X-gal staining of *R26*[CreERT2/R]; *Taf10*[flox/+] control at E9.5 (A), *R26*[+/R];*Taf10*[flox/flox] control at E10.5 (C) and E11.5 (E), and *R26*[CreERT2/R];*Taf10*[flox/flox] mutant at E9.5 (B), E10.5 (D) and E11.5 (F) after tamoxifen (tam) treatment at E7.5. (G) Western blot analysis of E9.5 *R26Cre;Taf10* whole embryos, treated (+) or not (−) with tamoxifen at E7.5, with anti-TAF10 or anti-histone H3 antibodies. (H,I) Confocal *z*-stack image projection of E9.25 *R26Cre;Taf10;Luvelu*/+ untreated (H) or tamoxifen-treated (I) embryos. so, somites. Scale bars: 500 μm in A-F; 100 μm in H,I.

Venus-PEST fusion. *Luvelu* expression is not affected in the absence of TAF10 at E9.5 (Fig. 1H,I), clearly indicating that transcription initiation still occurs in the *R26Cre;Taf10* mutant embryos, at least in the PSM. Altogether, these results show that, in mutants in which *Taf10* deletion is induced at E7.5, no TAF10 protein is detected in the PSM at E9.5, yet periodic gene transcription in the PSM is not affected.

Analyses of TFIID and SAGA composition in the absence of TAF10 in the mouse embryo
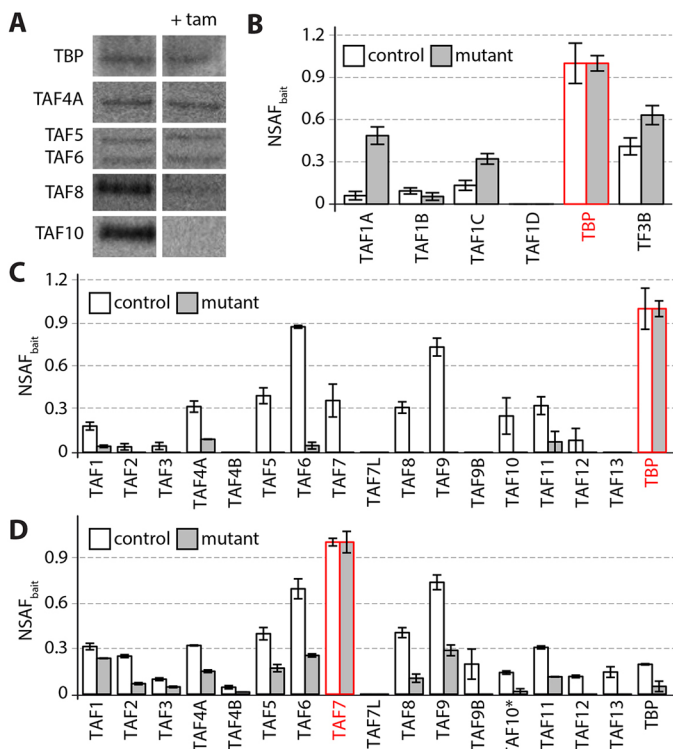
Next, we set out to analyze TFIID and SAGA composition by mass spectrometry in E9.5 mouse embryos, when no TAF10 protein is detected. To purify these complexes, we collected E9.5 embryos from $R26^{\mathrm{CreERT2/CreERT2}};Taf10^{\mathrm{flox/flox}} \times Taf10^{\mathrm{flox/flox}}$ crosses, treated (mutant) or not (control) with tamoxifen at E7.5. Complete *Taf10* deletion was assessed by PCR (data not shown) and western blot analysis, which confirmed the absence of detectable full-length TAF10 protein (Fig. 2A). Interestingly, in whole cell extracts from mutants, expression of TBP, TAF4A, TAF5 and TAF6 was not affected, whereas expression of TAF8, the main TFIID partner of TAF10, was strongly decreased (Fig. 2A), suggesting that the TAF8-TAF10 interaction is required for the stabilization of TAF8. We then compared TFIID and SAGA composition in the presence or absence of TAF10 by performing immunoprecipitations (IPs) from whole cell extracts of different TFIID and SAGA subunits using anti-TBP or anti-TAF7 antibodies (for TFIID) and with anti-TRRAP or anti-SUPT3 (for SAGA). Composition of the

Fig. 2. TFIID assembly defect in *R26Cre;Taf10* mutant embryos.
(A) Western blot analysis of the expression of TBP, TAF4A, TAF5, TAF6, TAF8 and TAF10 from whole cell extracts of E9.5 *R26Cre;Taf10* control (left, untreated) or mutant (right, treated with tamoxifen at E7.5) embryos. (B) TBP NSAF$_{\mathrm{bait}}$ values for SL1 complex subunits (TAF1A, TAF1B, TAF1C, TAF1D and TBP) and TF3B-TBP complex. (C,D) NSAF$_{\mathrm{bait}}$ values for TFIID subunits of TBP IP (C) and TAF7 IP (D). Bait proteins are indicated in red. Control and mutant IPs are indicated in white and gray, respectively. TAF10* corresponds to the full-length TAF10 protein. Error bars indicate s.d. *n*=3.

immunoprecipitated complexes was analyzed by mass spectrometry (Table S1). The normalized spectral abundance factor (NSAF) values were calculated for comparison of control and *Taf10* mutant samples (Zybailov et al., 2006).

In control embryos, the full-length TAF10 protein is represented by four peptides (Fig. S4A). In mutant embryo samples, no TAF10 peptides were detected in TBP and TRRAP IPs. By contrast, in TAF7 and SUPT3 IPs we detected significant amounts (albeit reduced compared with control) of the TAF10 N-terminal peptide (peptide #1; Fig. S4B,C). The $Taf10^{\mathrm{flox}}$ conditional mutation deletes exon 2, resulting in an out-of-frame fusion of exon 1 to exon 3 leading to premature truncation of TAF10 protein. This deletion is thus expected to produce a truncated N-terminal fragment of TAF10 containing peptide #1, but not the other peptides (Fig. S4D). The fact that no TAF10 peptides are detected in TBP and TRRAP IPs suggests that the truncated N-terminal peptide remaining in the mutant cannot participate in fully assembled TFIID or SAGA complexes. In addition, importantly, no TFIID subunits could be immunoprecipitated from murine $R26^{\mathrm{CreERT2/R}};Taf10^{\mathrm{flox/flox}}$ embryonic stem cells (ESCs), after 4-hydroxytamoxifen treatment, with an antibody that recognizes the N-terminal part of the TAF10 protein (Fig. S3B) and is able to immunoprecipitate the TFIID complex (Fig. S5A,B), showing that the truncated peptide is not part of a fully assembled TFIID complex. No conclusion could be drawn for the SAGA complex since this anti-N-terminal TAF10 antibody did not co-immunoprecipitate any of the mouse SAGA subunits even in control conditions (Fig. S5C). These data are consistent with the fact that the mutant truncated protein does not contain the HFD (Soutoglou et al., 2005). Thus, for further analyses and to score only the full-length protein we took into account peptides #2 to #4, which should be absent from the full-length TAF10 protein after deletion of the genomic sequences (TAF10*; Fig 2D, Fig. 3C, Fig. S4A,D), for TAF7 IPs (Fig. 2D) and SUPT3 IPs (Fig. 3C).
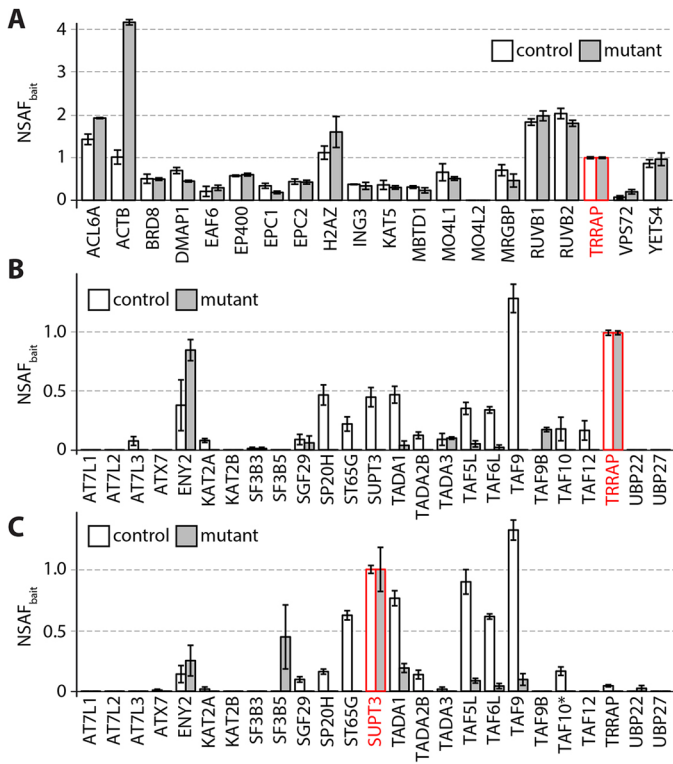
TBP is also part of SL1 and TFIIIB complexes, which are involved in Pol I and Pol III transcription, respectively (Vannini and Cramer, 2012). Importantly, TAF10 absence does not perturb the interaction of TBP with its non-TFIID partners, highlighting the lack of non-specific effects (Fig. 2B). In *Taf10* mutant embryos, we observed an increased interaction between TBP and the larger SL1 subunits TAF1A and TAF1C, suggesting that TBP might be redistributed in Pol I TAF-containing complexes in the absence of TAF10. This is consistent with the observation that there is no free TBP in the cells (Timmers and Sharp, 1991). In control TBP and TAF7 IPs, all the canonical TFIID subunits were detected (Fig. 2C,D). Interestingly, in *Taf10* mutant embryos, TBP IP reveals that TBP is mostly disengaged from TFIID, as only a few TAFs co-immunoprecipitate with TBP and in very low amounts (Fig. 2C). This TFIID dissociation is also observed in the TAF7 IP in the absence of TAF10 (Fig. 2D). Surprisingly, however, owing to the very efficient TAF7 IP (Table S1) we can still detect residual TFIID complexes (Fig. 2D). It is important to note that even if the anti-TAF7 antibody is able to co-immunoprecipitate several TAFs, TAF9B, TAF12 and TAF13 are not detected in the mutant, further supporting the conclusion that TAF10 absence strongly affects TFIID assembly.

In order to assess SAGA composition, we performed IPs against two SAGA subunits: SUPT3 and TRRAP. TRRAP is also a member of the chromatin remodeling complex TIP60/NuA4 (Sapountzi and Côté, 2011). As the interactions between TRRAP and TIP60/NuA4 subunits were not affected (Fig. 3A), we conclude that TAF10 absence does not interfere with the interactions between TRRAP and its non-SAGA partners. In both mutant TRRAP (Fig. 3B) and

**Fig. 3. SAGA assembly defect in _R26Cre;Taf10_ mutant embryos.**
(A) NSAF$_{bait}$ values for TIP60/NuA4 complex subunits of TRRAP IP from control or mutant extracts. (B,C) NSAF$_{bait}$ values for SAGA subunits of TRRAP IP (B) and SUPT3 IP (C) from control or mutant extracts. Bait proteins are indicated in red. TAF10* corresponds to the full-length TAF10 protein. Error bars indicate s.d. n=3.

SUPT3 (Fig. 3C) IPs we observed a dramatic reduction in the amount of SAGA subunits co-immunoprecipitated, clearly showing a defect in the assembly of SAGA. In contrast to TAF7 IP, we were not able to detect any residual canonical SAGA complexes in the mutant samples in the SUPT3-IP.

Altogether, these results strongly suggest that TAF10 is crucial for the assembly of both TFIID and SAGA in the mouse embryo, since the formation of both complexes is seriously impaired in _R26Cre;Taf10_ mutant embryos.

Taf10 conditional deletion in the paraxial mesoderm

Our next goal was to analyze the requirement for TAF10 in transcription during development. Somitogenesis is a dynamic developmental process in vertebrate embryos relying on periodic transcriptional waves sweeping from posterior to anterior in the PSM (Hubaud and Pourquié, 2014). As described above, the dynamic expression of the _Luvelu_ cyclic reporter is not affected in the PSM of E9.5 _R26Cre;Taf10_ mutant embryos (Fig. 1H,I). We carried out a _Taf10_ conditional deletion in the PSM using the _T-Cre_ line (Perantoni, 2005). This line expresses Cre in the primitive streak under the control of 500 bp of _T_ promoter sequence (Clements et al., 1996), leading to efficient recombination in the mesoderm before E7.5, including in paraxial mesoderm progenitors (Perantoni, 2005). _Taf10_ conditional deletion is embryonic lethal as no _T-Cre/+;Taf10_$^{flox/flox}$ (_T-Cre;Taf10_) mutants could be recovered at birth (data not shown). At E9.25, control and _T-Cre;Taf10_ mutant embryos are very similar, except that some mutant embryos show a curved trunk (Fig. 4A,B). At E10.25, _T-Cre;Taf10_ mutant embryos exhibit normal anterior development but show an apparent growth
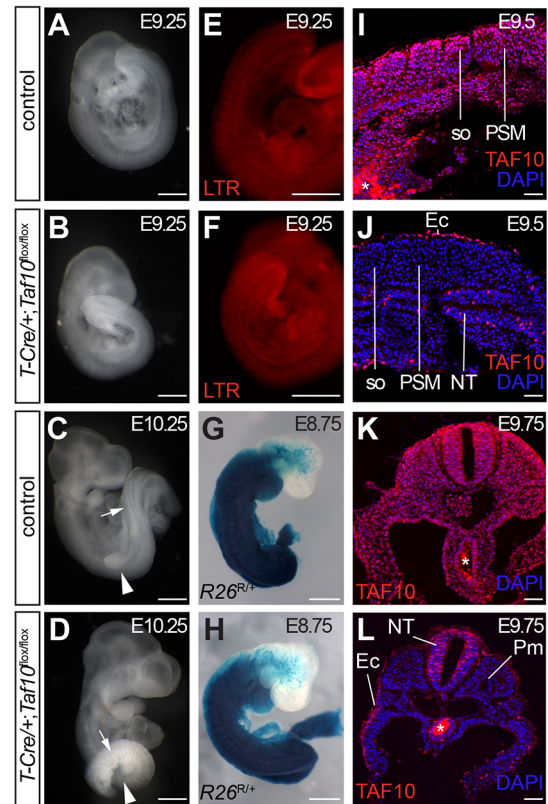
Fig. 4. Efficient _Taf10_ conditional deletion in the paraxial mesoderm.
(A-C) Whole-mount right-lateral view of control (A,C) and _T-Cre;Taf10_ mutant (B,D) embryos at E9.25 (A,B) and E10.25 (C,D). Arrowheads indicate the position of the forelimb bud that is absent in the mutant; arrows indicate the somites. (E,F) Cell death assay by LysoTracker Red (LTR) staining of E9.25 control (E) and _T-Cre;Taf10_ mutant (F) embryos. (G,H) Whole-mount X-gal staining of E8.75 _T-Cre/+;R26_$^{R/+}$ control (G) and _T-Cre/+;R26_$^{R/+}$;Taf10$^{flox/flox}$ mutant (H) embryos showing the efficient early recombination within the paraxial mesoderm. (I-L) DAPI counterstaining of TAF10 immunolocalization on E9.5 sagittal (I,J) and E9.75 transverse (K,L) sections from control (I,K) and _T-Cre;Taf10_ mutant (J,L) embryos. Asterisk indicates background due to secondary antibody trapping in the endoderm lumen. Ec, ectoderm; NT, neural tube; Pm, paraxial mesoderm; PSM, presomitic mesoderm; so, somites. Scale bars: 500 μm in A-H; 50 μm in I-L.

arrest of the trunk region, a helicoidal trunk lacking limb buds (Fig. 4C,D) and a degeneration of the allantois and placenta (data not shown). Whereas at E9.25 mutant and control somites were morphologically similar (Fig. 4A,B), E10.25 mutant somites were much smaller than the controls (Fig. 4C,D). Similar observations were made using the _Hes7-Cre_ line (data not shown), which has a similar recombination pattern in the mesoderm (Niwa et al., 2007). LysoTracker Red staining indicates that there is no obvious cell death in the mutants at E9.25 (Fig. 4E,F). Recombination in the mesoderm is efficient, as shown by the profile of activation of the Cre reporter allele _R26_^{R} at E8.75 (Fig. 4G,H). Full-length TAF10 protein expression could no longer be detected in the mesoderm of mutant embryos from as early as E8.5 (Fig. S6, Fig. 4I-L), including the PSM at E9.5 (Fig. 4I,J), whereas it is detected in the ectoderm. TAF10 expression was mosaic in the mutant neural tube (NT), which shares common progenitors with the mesoderm (Gouti et al., 2014; Tzouanacou et al., 2009). Surprisingly, these data show that there is a time window at ~E9.5 when embryonic development is not affected upon TAF10 depletion, except for the absence of limb buds, prior to an apparent growth arrest and decay at E10.5.

Absence of TAF10 in the PSM does not affect somitogenesis at E9.5

To gain more insight into somitogenesis, we compared somite numbers between the different genotypes at E9.5 (Fig. 5A). Although no significant statistical differences could be detected, mutant embryos tended to have half a somite less than the other genotypes. This could be explained by a slowing down of somitogenesis at late E9.5 stage.

We next analyzed the expression of specific PSM markers using WISH. Expression of the posterior PSM marker *Msgn1* (Wittler et al., 2007) (Fig. 5B,C), the segmentation gene *Mesp2* (Saga et al., 1997) (Fig. 5D,E) or the caudal somite marker *Uncx4.1* (Neidhardt et al., 1997) (Fig. 5F,G) was unaffected in the absence of TAF10. WISH of cyclic genes of the Notch [*Lfng* (Forsberg et al., 1998; McGrew et al., 1998) and *Hes7* (Bessho et al., 2003); Fig. 5H,I, Fig. S8A,B], Wnt [*Axin2* (Aulehla et al., 2003); Fig. S7C,D] or FGF [*Snai1* (Dale et al., 2006); Fig. S7E,F] pathways revealed that the different phases of expression could be observed in *T-Cre;Taf10* mutant embryos. Altogether, the rhythmic transcription of the cyclic genes in the absence of TAF10 suggests that active transcription proceeds normally in the PSM of mutant embryos.

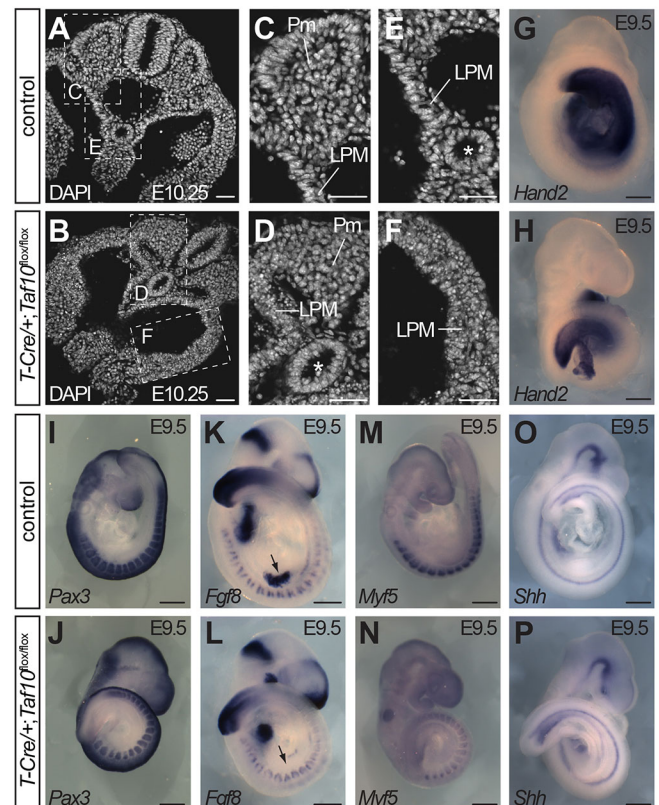## Absence of TAF10 differentially affects mesoderm derivatives

Limb bud outgrowth requires signals such as FGF8 from the apical ectodermal ridge (AER), which controls proliferation of the underlying mesenchyme derived from the lateral plate mesoderm (LPM) (Zeller et al., 2009). On E10.25 transverse sections from control embryos, mesodermal nuclei (including those in the LPM) are regularly shaped (Fig. 6A,C,E). In *T-Cre;Taf10* mutants

(Fig. 6B) the paraxial mesoderm nuclei appear normal (Fig. 6D), whereas in the LPM [and in the intermediate mesoderm (data not shown)] we observed massive nuclear fragmentation characterized by the presence of pyknotic nuclei (Fig. 6F). Since we did not observe any difference in the efficiency of TAF10 protein depletion between the paraxial mesoderm and the LPM from as early as E8.5 (Fig. S6), these data indicate that the LPM is more sensitive to *Taf10* loss than the paraxial mesoderm.

We carried out WISH in order to test whether *Taf10* loss differentially affects the expression of specific markers of the different types of mesoderm. Expression of the LPM marker *Hand2* (Fernandez-Teran et al., 2000) is clearly downregulated in the mutants (Fig. 6G,H). Similar observations were made with *Prdm1*, which is expressed in the growing mesenchyme during limb bud outgrowth (Vincent et al., 2005) (data not shown). The absence of *Fgf8* induction in the presumptive AER in E9.5 *T-Cre;Taf10* mutant embryos (Fig. 6K,L) indicates that the LPM defect is early and probably precedes the cell death in this tissue, since no obvious cell death could be detected at E9.25 (Fig. 4F). The cell death observed later on in the LPM is, however, not caused by the lack of *Fgf8* expression as it is also observed at non-limb levels. By contrast, paraxial mesoderm marker analysis shows that *Pax3* expression in the anterior PSM and early somites (Goulding et al., 1991) is normal (Fig. 6I,J). Similarly, *Fgf8* expression domains in the rostral and
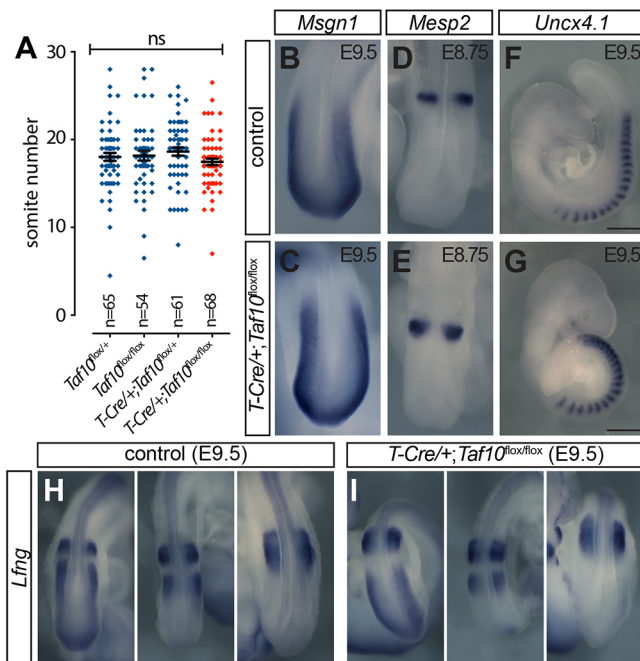
Fig. 5. Absence of TAF10 in the PSM does not affect segmentation.
(A) Somite number quantification (one-way ANOVA; ns, non significant). Error bars indicate s.e.m. and the middle bar indicates the mean. (B-I) WISH of E9.5 (B,C,F-I) and E8.75 (D,E) control (B,D,F,H) and *T-Cre/+;Taf10*flox/flox mutant (C,E,G,I) embryos for the posterior PSM marker *Msgn1* (B,C), the segmentation gene *Mesp2* (D,E), the caudal somite marker *Uncx4.1* (F,G) and the cyclic gene *Lfng* (H,I). Dorsal tail tip (B-E,H,I) or right-lateral (F,G) views are presented. Scale bars: 100 µm in B-E,H,I; 500 µm in F,G.

Fig. 6. Absence of TAF10 differentially affects the different types of mesoderm. (A-F) DAPI-stained transverse sections of E10.25 control (A, magnified in C,E) and *T-Cre/+;Taf10*flox/flox mutant (B, magnified in D,F) embryos showing nuclear fragmentation in LPM but normal nuclear morphology in the paraxial mesoderm. Asterisks indicate the endoderm. (G-P) WISH of E9.5 control (G,I,K,M,O) and *T-Cre/+;Taf10*flox/flox mutant (H,J,L,N,P) embryos for *Hand2* (G,H), *Pax3* (I,J), *Fgf8* (K,L), *Myf5* (M,N) and *Shh* (O,P). Arrows indicate the apical ectodermal ridge. LPM, lateral plate mesoderm; Pm, paraxial mesoderm. Scale bars: 50 µm in A-F; 500 µm in G-P.

caudal lips of the dermomyotome (Crossley and Martin, 1995) are not affected at E9.5 in the mutant paraxial mesoderm (Fig. 6K,L). Expression of *Pax3* in the dermomyotome (Goulding et al., 1991) and of *Myf5* in the myotome (Ott et al., 1991) are however decreased in *T-Cre;Taf10* mutants (Fig. 6I,J,M,N). Defective myotome formation was evidenced by immunolocalization of myogenin or myosin heavy chains at E9.5 and E10.5 (data not shown). Similar observations were made in *Hes7-Cre/+;Taf10*flox/flox mutant embryos (Fig. S8). Expression of *Shh* in the notochord is normal (Echelard et al., 1993), indicating that the axial mesoderm is not obviously affected in *T-Cre;Taf10* mutant embryos (Fig. 6O,P). Altogether, these results indicate different requirements for TAF10 depending on the type of mesoderm. However, we cannot rule out the possibility that the effect seen in the LPM arises secondarily to a defect in the developing paraxial mesoderm.

Absence of TAF10 does not affect global steady-state mRNA and cyclic transcription in the PSM

Our next goal was to investigate Pol II transcription status in mutant embryos. We first compared steady-state rRNA (Pol I) and mRNA (Pol II) transcript levels by quantifying the absolute expression levels of 18S ribosomal RNA (*Rn18s*) versus classical Pol II housekeeping genes (*Actc1*, *Gapdh* and *Rplp0*) (Fig. 7A). No significant differences between mutant and control samples were detected when comparing the results obtained with three different pairs of *Rn18s* primers (Fig. 7B). The results were similar for *Gapdh* and *Rplp0* (Fig. 7B). Expression of the *Luvelu* reporter (Aulehla et al., 2008) in *T-Cre;Taf10* mutant embryos (Fig. 7C,D) supports the idea that cyclic transcription initiation still occurs in the *T-Cre;Taf10* mutant PSM at E9.5. Altogether, these results indicate that, at ~E9.5, absence of detectable TAF10 does not affect global steady-state mRNA and PSM-specific cyclic transcription.

Expression of specific genes is altered in the PSM at E9.5 in the absence of TAF10

We next performed a transcriptome analysis in order to see whether specific genes were affected in the absence of TAF10. We performed microarray analyses from microdissected PSMs of E9.5 (17-19 somites) control and *T-Cre;Taf10* mutant embryos (Fig. 8A). Analysis by scatter plot shows that TAF10 loss has only a very minor impact on gene expression (Fig. 8B). We then performed a statistical analysis using fold change ranking ordered statistics (FCROS) (Dembélé and Kastner, 2014) and found 369 differentially expressed genes (218 downregulated and 151 upregulated) using a fold change cut-off of 1.5 (Fig. 8C, see Table S2). This analysis identified genes related to the cell cycle, TAFs, signaling pathways, and Hox/para-Hox genes (see Table 1). We also observed that some genes previously identified as cyclic genes in the PSM, such as *Egr1*, *Cyr61*, *Dkk1*, *Spry4* and *Rps3a* (Krol et al., 2011), are also differentially expressed in *T-Cre;Taf10* mutant PSMs (Table 1, Fig. S9A). Interestingly, the most highly upregulated gene (4.8-fold) is *Cdkn1a*, which encodes a cyclin-dependent kinase inhibitor involved in G1 arrest (Dulić et al., 1994). We identified *Gas5*, a tumor suppressor gene that encodes two long non-coding RNAs and several small nucleolar RNAs in its introns (Ma et al., 2015), as the most downregulated gene (−2- to −4.9-fold). We confirmed the upregulation of *Cdkn1a*, *Cdkn1c*, *Ccng1* and *Cdkl3* and the downregulation of *Gas5* by RT-qPCR using control and *T-Cre;Taf10* mutant tail tips (Fig. 8D). Upregulation of *Cdkn1a* and *Cdkn1c* could explain the growth arrest that is observed in *T-Cre;Taf10* mutant embryos.
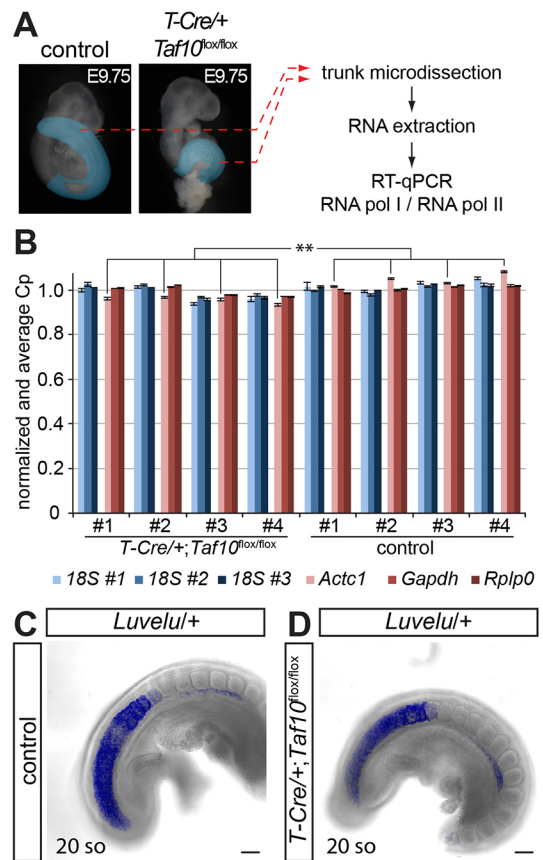

Fig. 7. Global transcription is not affected in the absence of TAF10 in the paraxial mesoderm. (A) Comparison between Pol II and Pol I transcription. The trunk axial structures highlighted in blue were dissected from E9.75 control and *T-Cre/+;Taf10*flox/flox mutant embryos and RT-qPCR was performed for Pol I-specific and Pol II-specific housekeeping genes. (B) Comparison of averaged and normalized expression of Pol I-specific (blue) and Pol II-specific (red) markers from control (right side) and mutant (left side) samples. **P<0.01 (Aspin-Welch corrected Student's t-test). Error bars indicate s.e.m. n=4. (C,D) Confocal z-stack image projection of E9.5 *Luvelu*/+ control (C) and *T-Cre/+; Taf10*flox/flox;*Luvelu*/+ mutant (D) embryos. so, somites. Scale bars: 100 µm.

Some TFIID-TAFs were also upregulated: *Taf5* (1.5-fold), *Taf6* (1.7-fold) and *Taf9b* (1.6-fold) (Table 1, Table S2). We validated these differential expressions by RT-qPCR and found that most of the genes encoding the other TAFs were also upregulated (Fig. S9B). The biological significance of these differences is not clear as no obvious increase in protein levels could be observed for TAF4A, TAF5 and TAF6 (Fig. 2A). *Taf10* expression is downregulated in *T-Cre;Taf10* mutant tail tips, as is that of *Taf8*, which encodes the main partner of TAF10 in TFIID. These data suggest that the decreased level of TAF8 protein observed in *R26Cre;Taf10* lysates (Fig. 2A) could also be related to transcriptional regulation. No differences could be detected for the SAGA-specific TAF5L and TAF6L (Fig. S9C). Altogether, our data show that, in the PSM at E9.5, gene expression controlled by Pol II is not globally affected in the absence of TAF10; however, the lack of TAF10 could induce a change in the steady-state mRNA levels of specific genes.

DISCUSSION

The composition of TFIID and SAGA complexes in the developing mouse embryo has not yet been described. Here, we analyzed the composition of these complexes in E9.5 mouse embryos in the
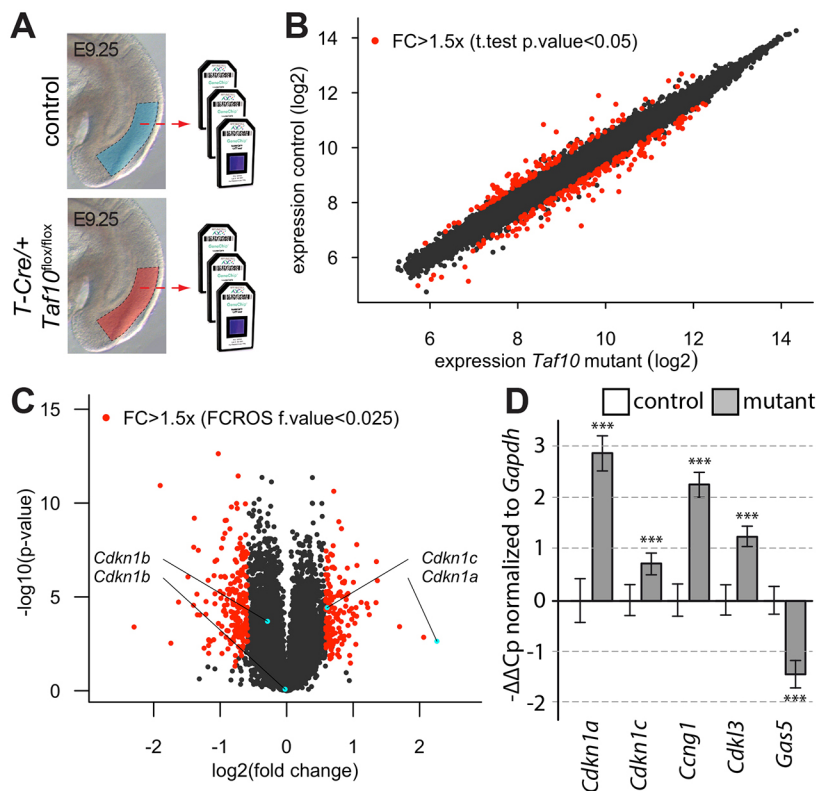
Fig. 8. A limited specific effect on Pol II transcription in the absence of TAF10 in the PSM. (A) Strategy used for the microarray analysis from E9.5 microdissected PSM of control (blue) and *T-Cre;Taf10* mutant (red) embryos. (B) Scatter plot comparing gene expression between control and *T-Cre;Taf10* mutant PSM. Red dots correspond to statistically significant differences for a fold change greater than 1.5 after *t*-test. (C) Volcano plot comparing gene expression between control and *T-Cre/+;Taf10*flox/flox mutant PSM after FCROS analysis. Red dots correspond to statistically significant differences for a fold change greater than 1.5. (D) RT-qPCR analysis for cell cycle genes from E9.25 control and *TCre;Taf10* mutant tail tips. −ΔΔCp values are normalized to *Gapdh*. ***$P<0.001$ (Aspin-Welch corrected Student's *t*-test). Error bars indicate s.e.m. *n*=4.

presence and absence of TAF10. We showed that the absence of TAF10 strongly affects TFIID and SAGA formation. *Taf10* deletion during somitogenesis confirmed the requirement of TAF10 during embryonic development in agreement with previous studies (Indra et al., 2005; Mohan et al., 2003; Tatarakis et al., 2008). However, in contrast to these studies, we identified a time window at ~E9.5 when no obvious somitogenesis defects are detected, despite the absence of detectable full-length TAF10 protein in mutant embryos. In these mutants, transcription is still broadly functional as shown by the lack of any global effect on Pol II transcription.

TAF10 is required for TFIID and SAGA assembly during development

Our data demonstrate a global decrease in TFIID and SAGA assembly in *Taf10* mutant embryos. In F9 cells, in the absence of TAF10, TFIID is minimally affected by the release of TBP from the complex, while interaction between the different TAFs is maintained (Mohan et al., 2003), whereas in the liver TFIID assembly is completely abrogated (Tatarakis et al., 2008). These differences could be explained either by cell type-specific differences or by a difference in the timing of these analyses following *Taf10* deletion, as Tatarakis et al. (2008) performed their experiments 8-15 days after *Taf10* deletion. The status of SAGA has not previously been investigated in *Taf10* mutant embryos. Our work demonstrates for the first time that not only TFIID, but also SAGA is affected in *Taf10* mutant embryos. Our new data show that the defect in the assembly of canonical TFIID and SAGA is already observed 2 days after the induction of *Taf10* deletion, a timing that coincides with the disappearance of detectable full-length TAF10 protein. On the other hand, we can still detect reduced interactions between TAF7 and several TAFs following *Taf10* deletion suggesting that, as observed in HeLa or F9 cells, there could be some TFIID-like complexes that do not contain TAF10, albeit in

reduced levels. Our data exclude the existence of similar TAF10-less SAGA-like complexes in the embryo.

TAF10 depletion is very efficient since no TAF10 proteins can be detected by western blot in the mutant embryo lysates. Analysis of the detected peptides strongly suggests that it is only in the TAF7 IP (TFIID) that potential full-length TAF10 proteins are detected, albeit at very low frequency. This suggests that very low levels of canonical TFIID complexes could still be present at E9.5 in the mutant embryonic lysates. Furthermore, these results, in comparison with the SAGA IPs, suggest that TAF10 is very stable when incorporated into TFIID, probably because of the lower rate of TFIID turnover compared with that of SAGA.

TFIID is built from submodules that assemble in the cytoplasm, at least *in vitro* (Bieniossek et al., 2013; Trowitzsch et al., 2015), and it is likely that such TFIID submodules are immunoprecipitated in our experiments since we performed our analyses using whole cell extracts. The TAF7 paralog TAF7L, which has been associated with germ cells and adipocytes (Zhou et al., 2013a,b), is not present in TFIID IPs, indicating that the majority of TFIID contains TAF7, at least at E9.5. However, other TAF paralogs such as TAF4A and TAF4B, TAF9 and TAF9B, are detected. This potential TFIID diversity could exist inside all the cells or could be cell type specific and could explain the developmental differences observed between LPM and paraxial mesoderm. However, novel methods will be required to characterize the composition of TFIID and SAGA complexes in a cell type-specific manner in the embryo.

A truncated TAF10 protein can potentially be integrated into TFIID and SAGA submodules

Our strategy conditionally removes exon 2 and theoretically leads to the splicing of exon 1 to exon 3 (Mohan et al., 2003). These exons are not in frame and therefore the 77 amino acids coded by exon 1 are followed by 15 extra amino acids in the mutant

DEVELOPMENT

Table 1. Selection of differentially expressed genes in the PSM of E9.5 *T-Cre;Taf10* mutant embryos

Description	Gene symbol	Absolute FC	*F*-value
Cell cycle			
growth arrest specific 5	*Gas5*	−4.908	0.0177
		−3.736	0.0178
		−2.635	0.0179
		−2.073	0.0183
cyclin-dependent kinase inhibitor 1A (P21)	*Cdkn1a*	4.790	0.9820
cyclin-dependent kinase inhibitor 1C (P57)	*Cdkn1c*	1.525	0.9795
cyclin-dependent kinase-like 3	*Cdkl3*	1.780	0.9811
cyclin G1	*Ccng1*	2.006	0.9817
RNA pol I-associated complexes			
TATA box binding protein (Tbp)-associated factor, RNA polymerase I, D	*Taf1d*	−2.317	0.0181
		−2.266	0.0181
		−2.040	0.0186
		−1.790	0.0193
		−1.632	0.0204
RNA pol II-associated complexes			
TAF6 RNA polymerase II, TATA box binding protein (TBP)-associated factor	*Taf6*	1.724	0.9809
TAF9B RNA polymerase II, TATA box binding protein (TBP)-associated factor	*Taf9b*	1.591	0.9786
TAF5 RNA polymerase II, TATA box binding protein (TBP)-associated factor	*Taf5*	1.536	0.9788
polymerase (RNA) II (DNA directed) polypeptide A	*Polr2a*	1.505	0.9792
Signaling pathways and transcription factors			
Mix1 homeobox-like 1 (*Xenopus laevis*)	*Mixl1*	1.566	0.9787
T-box 6	*Tbx6*	1.547	0.9799
E26 avian leukemia oncogene 2, 3′ domain	*Ets2*	−1.538	0.0217
fibroblast growth factor 9	*Fgf9*	−1.550	0.0215
ephrin A5	*Efna5*	−1.628	0.0208
dual specificity phosphatase 4	*Dusp4*	−1.648	0.0202
R-spondin 3 homolog (*Xenopus laevis*)	*Rspo3*	−1.662	0.0200
cytochrome P450, family 26, subfamily a, polypeptide 1	*Cyp26a1*	−1.671	0.0206
caudal type homeobox 4	*Cdx4*	−1.519	0.0232
homeobox A7	*Hoxa7*	1.636	0.9806
homeobox B7	*Hoxb7*	1.823	0.9814
homeobox D1	*Hoxd1*	1.971	0.9817
homeobox A3	*Hoxa3*	2.550	0.9820
Cyclic genes			
early growth response 1	*Egr1*	1.610	0.9791
cysteine rich protein 61	*Cyr61*	1.713	0.9810
dickkopf homolog 1 (*Xenopus laevis*)	*Dkk1*	1.945	0.9811
sprouty homolog 4 (*Drosophila*)	*Spry4*	−1.539	0.0219
ribosomal protein S3A	*Rps3a*	−1.586	0.0209

Statistical analysis was performed using FCROS with a cut-off of 1.5 for the fold change (FC). Difference is considered significant for an *F*-value below 0.025 or above 0.975. Where multiple entries appear for the same gene, each corresponds to a different specific probe set.

(Fig. S4D). This mutant protein has the N-terminal unstructured domain of TAF10 but, more importantly, lacks its HFD required for the interaction with TAF3, TAF8 or SUPT7L/ST65G (Soutoglou et al., 2005). HFD-HFD interactions are crucial for nuclear import of TAF10, which does not contain any NLS (Soutoglou et al., 2005). Since no TFIID subunits could be co-immunoprecipitated from whole cell extracts of *R26*[CreERT2/R]*;Taf10*[flox/flox] ESCs, after 4-hydroxytamoxifen treatment, with an antibody that recognizes the N-terminal part of TAF10 (Fig. S5), it is very unlikely that this truncated protein can be incorporated into mature SAGA and TFIID

complexes that are functional in the nucleus. However, we cannot rule out the possibility that this truncated protein could be incorporated into rare cytoplasmic submodules containing TAF7 or SUPT3. Nevertheless, because the *Taf10* mutant heterozygotes are indistinguishable from control embryos (Fig. 1A), this also argues against a dominant-negative effect of this peptide.

Another interesting question is the functionality of these potentially partial TFIID and/or SAGA complexes that are fully depleted of TAF10 protein or contain the truncated TAF10. From our data, it is obvious that these different partial complexes cannot fully compensate for the loss of wild-type complexes, but one cannot rule out a partial activity. Future analyses of the difference between the different types of mesoderm could help to elucidate whether such partial non-canonical TFIID and/or SAGA complexes have activities.

Differential sensitivity to *Taf10* loss in the mesoderm

Taf10 deletion in the mesoderm or in the whole embryo leads to developmental arrest that could be explained by the upregulation of *Cdkn1a* and *Cdkn1c* expression. Similar observations were made in yeast (Kirschner et al., 2002) and in F9 cells (Metzger et al., 1999) following depletion of TAF10. Surprisingly, we also observed the downregulation of the tumor suppressor *Gas5*, which is associated with increased proliferative and anti-apoptosis effects in cancer cells (Pickard and Williams, 2015). Interestingly, *Cdkn1a* expression is positively controlled by *Gas5* in stomach cancer at the transcript and protein levels (Liu et al., 2015). It is thus possible that TAF10 is required for the correct functioning of the *Gas5* regulatory network during development.

The phenotypes of null mutations in genes encoding TFIID-TAFs, such as *Taf7* (Gegonne et al., 2012) or *Taf8* (Voss et al., 2000), are very similar to that of the *Taf10* mutant (Mohan et al., 2003). In particular, these mutations are embryonic lethal around implantation stage. Moreover, *Taf7* null MEFs stop proliferating, suggesting that the growth arrest observed in our mutants is a direct consequence of the failure to properly build TFIID. We cannot exclude a potential contribution of SAGA loss in our mutants. However, deletion of genes coding for different enzymatic activities of SAGA such as *Kat2a;Kat2b* or *Usp22* are embryonic lethal, but with phenotypes much less severe than that of *Taf10* mutation (Lin et al., 2012; Xu et al., 2000; Yamauchi et al., 2000). Interestingly, axial and paraxial mesoderm formation are affected in *Kat2a;Kat2b* mutants, whereas extraembryonic and cardiac mesoderm formation are not (Xu et al., 2000), strongly suggesting that SAGA could also have different functions in different types of mesoderm.

Another striking observation is that, although no TAF10 protein could be detected as early as E8.5 in the mesoderm of *T-Cre;Taf10* mutant embryos, we observed a difference in sensitivity to *Taf10* loss between the LPM (and the intermediate mesoderm) and the paraxial mesoderm. We observed a very early defect in the LPM, with strong downregulation of specific markers and absence of limb bud outgrowth. The absence of limb buds could be explained by a defect in FGF10 signaling activation in the mesoderm and/or by cell death in the LPM that occurs earlier than in the paraxial mesoderm of *T-Cre;Taf10* mutants. The relative resistance of the mutant paraxial mesoderm to cell death also suggests a difference of sensitivity. A similar observation has been made in F9 cells, where RA-induced differentiation of F9 cells into primitive endoderm rescued the apoptosis of *Taf10* mutant cells (Metzger et al., 1999). This effect was not observed when F9 cells were differentiated into parietal endoderm in the presence of RA and cAMP (Metzger et al., 1999). An interesting possibility is that, being the principal source

of RA (Niederreither et al., 1997), the paraxial mesoderm is protected from cell death in the mutant embryos via an autocrine mechanism. A difference in sensitivity has also been observed in *Taf10* mutant blastocysts, where the inner cell mass dies by apoptosis, whereas trophoblast can be maintained in culture (Mohan et al., 2003). It is interesting to note that trophoblast, primitive and parietal endoderms are extraembryonic structures and are not part of the fully developed embryo. This is the first *in vivo* observation of a difference in sensitivity to the loss of *Taf10* in an embryonic lineage. Since *Taf10* was deleted in paraxial mesoderm and LPM progenitors, we cannot rule out the possibility that the increased sensitivity of the LPM is indirect and mediated by the paraxial mesoderm, although we did not observe any obvious change in gene expression in the PSM at a time when limb bud development is already affected. Nevertheless, a tempting speculation is that TAF10 could serve as an interface of interaction with an LPM-specific transcription factor, as has been described recently for GATA1 during erythropoiesis (Papadopoulos et al., 2015).

MATERIALS AND METHODS

Mice
Animal experimentation was carried out according to animal welfare regulations and guidelines of the French Ministry of Agriculture (ethical committee C2EA-17 projects 2012-077, 2012-078, 2015050509092048). All the lines have already been described (supplementary Materials and Methods). The day of vaginal plug was scored as embryonic day (E) 0.5. Tamoxifen (Sigma) resuspended at 20 mg/ml in 5% ethanol/filtered sunflower seed oil was injected intraperitoneally [150 µl (3 mg) for a 20 g mouse] at E7.5.

Embryos whole cell extracts
E9.5 mouse embryos (16-20 somites) were lysed in 10% glycerol, 20 mM Hepes pH 7, 0.35 M NaCl, 1.5 mM $MgCl_2$, 0.2 mM EDTA, 0.1% Triton X-100 with protease inhibitor cocktail (PIC, Roche) on ice. Lysates were treated three times with a pestle stroke followed by three liquid nitrogen freeze-thaw cycles. Lysates were centrifuged at 20,817 rcf for 15 min at 4°C and the supernatants were used directly for IPs or stored at −80°C for western blots.

Immunoprecipitations
Inputs were incubated with Dynabeads coated with antibodies (see supplementary Materials and Methods and Table S3) overnight at 4°C. Immunoprecipitated proteins were washed twice for 5 min each with 500 mM KCl buffer [25 mM Tris-HCl (pH 7), 5 mM $MgCl_2$, 10% glycerol, 0.1% NP40, 2 mM DTT, 500 mM KCl and PIC (Roche)], then washed twice for 5 min each with 100 mM KCl buffer (25 mM Tris-HCl pH 7, 5 mM $MgCl_2$, 10% glycerol, 0.1% NP40, 2 mM DTT, 100 mM KCl and PIC) and eluted with 0.1 M glycine pH 2.8 three times for 5 min each. Elution fractions were neutralized with 1.5 M Tris-HCl pH 8.8.

Western blots
Immune complexes or 15 µg embryo lysates were boiled for 10 min in 100 mM Tris-HCl pH 6.8, 30% glycerol, 4% SDS, 0.2% Bromophenol Blue, 100 mM DTT, resolved on a precast SDS-polyacrylamide gel 4-12% (Novex) and transferred to nitrocellulose membrane (Protran, Amersham). Membranes were blocked in 3% milk in PBS for 30 min and incubated with primary antibody (Table S3) overnight at 4°C. Membranes were washed three times for 5 min each with 0.05% Tween 20 in PBS. Membranes were incubated with HRP-coupled secondary antibodies (Table S3) for 50 min at room temperature, followed by ECL detection (ThermoFisher Scientific).

Mass spectrometry analyses
Samples were analyzed using an UltiMate 3000 RSLCnano (Thermo Scientific) coupled in line with a linear trap Quadrupole (LTQ)-Orbitrap ELITE mass spectrometer via a nano-electrospray ionization source

(Thermo Scientific). Data were analyzed by calculation of $NSAF_{bait}$ (see supplementary Materials and Methods).

Section and immunolocalization
Embryos were fixed in 4% paraformaldehyde for 2 h at 4°C, rinsed three times in PBS, equilibrated in 30% sucrose/PBS and embedded in Cryomatrix (Thermo Scientific) in liquid nitrogen vapors. Sections (20 µm) were obtained on a Leica cryostat. Immunolabeling was performed as previously described (Vincent et al., 2014). Sections were counterstained with DAPI (4′,6-diamidino-2-phenylindole dihydrochloride; Molecular Probes) and imaged with an LSM 510 laser-scanning microscope (Carl Zeiss) and 20× Plan APO objective (NA 0.8).

Luvelu imaging
Freshly dissected embryos were kept in DMEM without Phenol Red (Life Technologies). Luvelu signal was detected using an SP5 TCS confocal microscope (Leica) with a 20× Plan APO objective (NA 0.7).

Whole-mount *in situ* hybridization (WISH), X-gal and LysoTracker Red staining
WISH was performed as described (Nagy et al., 2002). *Axin2*, *Fgf8*, *Hand2*, *Lfng*, *Msgn1*, *Myf5*, *Shh*, *Snai1* and *Uncx4.1* probes have been described (Aulehla and Johnson, 1999; Aulehla et al., 2008; Crossley and Martin, 1995; Dale et al., 2006; Echelard et al., 1993; Mansouri et al., 1997; Ott et al., 1991; Srivastava et al., 1997; Yoon et al., 2000). A minimum of three embryos were used for the classical markers and a minimum of seven embryos were used for the cyclic genes. X-gal and LysoTracker Red (Molecular Probes) stainings were performed as described (Rocancourt et al., 1990; Vincent et al., 2014).

RT-qPCR and statistical analysis
Microdissected embryo tail tip or trunk tissue (without limb buds for the controls) was lysed in 500 µl TRIzol (Life Technologies). RNA was extracted according to the manufacturer's recommendations and resuspended in 20 µl (trunk) or 11 µl (tail tips) RNase-free water (Ambion). Reverse transcription was performed using the QuantiTect Reverse Transcription Kit (Qiagen) in 12 µl reaction volume and diluted by adding 75 µl RNase-free water. Quantitative PCRs were performed on a Roche LightCycler II 480 using LightCycler 480 SYBR Green I Master (Roche) in 8 µl reaction volume (0.4 µl cDNA, 0.5 µM primers). Four mutants and four controls with the same somite number were analyzed in triplicate. Statistical analysis and primer sequences are described in the supplementary Materials and Methods and Table S4.

Microarray and statistical analysis
Posterior PSMs of E9.5 embryos were individually microdissected (Dequéant et al., 2006) and lysed in 200 µl TRIzol, and the yolk sac was used for genotyping. Three PSMs of 17- to 19-somite embryos of the same genotype were pooled for one replicate and analyzed on GeneChip MoGene 1.0 ST arrays (Affymetrix). Data were normalized using RMA (Bioconductor), filtered, and FCROS (Dembélé and Kastner, 2014) was used for the statistical analysis (supplementary Materials and Methods).

DEVELOPMENT

Data availability
Raw microarray data have been deposited in Gene Expression Omnibus under accession number GSE82186. Raw mass spectrometry data are available via ProteomeXchange under accession number PXD004688.

Supplementary information
Supplementary information available online at
http://dev.biologists.org/lookup/doi/10.1242/dev.146902.supplemental

References
Aulehla, A. and Johnson, R. L. (1999). Dynamic expression of lunatic fringe suggests a link between notch signaling and an autonomous cellular oscillator driving somite segmentation. *Dev. Biol.* **207**, 49-61.
Aulehla, A., Wehrle, C., Brand-Saberi, B., Kemler, R., Gossler, A., Kanzler, B. and Herrmann, B. G. (2003). Wnt3a plays a major role in the segmentation clock controlling somitogenesis. *Dev. Cell* **4**, 395-406.
Aulehla, A., Wiegraebe, W., Baubet, V., Wahl, M. B., Deng, C., Taketo, M., Lewandoski, M. and Pourquié, O. (2008). A beta-catenin gradient links the clock and wavefront systems in mouse embryo segmentation. *Nat. Cell Biol.* **10**, 186-193.
Bessho, Y., Hirata, H., Masamizu, Y. and Kageyama, R. (2003). Periodic repression by the bHLH factor Hes7 is an essential mechanism for the somite segmentation clock. *Genes Dev.* **17**, 1451-1456.
Bieniossek, C., Papai, G., Schaffitzel, C., Garzoni, F., Chaillet, M., Scheer, E., Papadopoulos, P., Tora, L., Schultz, P. and Berger, I. (2013). The architecture of human general transcription factor TFIID core complex. *Nature* **493**, 699-702.
Bonnet, J., Wang, C.-Y., Baptista, T., Vincent, S. D., Hsiao, W.-C., Stierle, M., Kao, C.-F., Tora, L. and Devys, D. (2014). The SAGA coactivator complex acts on the whole transcribed genome and is required for RNA polymerase II transcription. *Genes Dev.* **28**, 1999-2012.
Clements, D., Taylor, H. C., Herrmann, B. G. and Stott, D. (1996). Distinct regulatory control of the Brachyury gene in axial and non-axial mesoderm suggests separation of mesoderm lineages early in mouse gastrulation. *Mech. Dev.* **56**, 139-149.
Cole, S. E., Levorse, J. M., Tilghman, S. M. and Vogt, T. F. (2002). Clock regulatory elements control cyclic expression of Lunatic fringe during somitogenesis. *Dev. Cell* **3**, 75-84.
Crossley, P. H. and Martin, G. R. (1995). The mouse Fgf8 gene encodes a family of polypeptides and is expressed in regions that direct outgrowth and patterning in the developing embryo. *Development* **121**, 439-451.
Dale, J. K., Malapert, P., Chal, J., Vilhais-Neto, G., Maroto, M., Johnson, T., Jayasinghe, S., Trainor, P., Herrmann, B. and Pourquié, O. (2006). Oscillations of the snail genes in the presomitic mesoderm coordinate segmental patterning and morphogenesis in vertebrate somitogenesis. *Dev. Cell* **10**, 355-366.
Dembélé, D. and Kastner, P. (2014). Fold change rank ordering statistics: a new method for detecting differentially expressed genes. *BMC Bioinformatics* **15**, 14.
Dequéant, M.-L., Glynn, E., Gaudenz, K., Wahl, M., Chen, J., Mushegian, A. and Pourquié, O. (2006). A complex oscillating network of signaling genes underlies the mouse segmentation clock. *Science* **314**, 1595-1598.
Dulić, V., Kaufmann, W. K., Wilson, S. J., Tisty, T. D., Lees, E., Harper, J. W., Elledge, S. J. and Reed, S. I. (1994). p53-dependent inhibition of cyclin-dependent kinase activities in human fibroblasts during radiation-induced G1 arrest. *Cell* **76**, 1013-1023.
Echelard, Y., Epstein, D. J., St-Jacques, B., Shen, L., Mohler, J., McMahon, J. A. and McMahon, A. P. (1993). Sonic hedgehog, a member of a family of putative signaling molecules, is implicated in the regulation of CNS polarity. *Cell* **75**, 1417-1430.
Fernandez-Teran, M., Piedra, M. E., Kathiriya, I. S., Srivastava, D., Rodriguez-Rey, J. C. and Ros, M. A. (2000). Role of dHAND in the anterior-posterior polarization of the limb bud: implications for the Sonic hedgehog pathway. *Development* **127**, 2133-2142.
Forsberg, H., Crozet, F. and Brown, N. A. (1998). Waves of mouse Lunatic fringe expression, in four-hour cycles at two-hour intervals, precede somite boundary formation. *Curr. Biol.* **8**, 1027-1030.

Gegonne, A., Tai, X., Zhang, J., Wu, G., Zhu, J., Yoshimoto, A., Hanson, J., Cultraro, C., Chen, Q.-R., Guinter, T. et al. (2012). The general transcription factor TAF7 is essential for embryonic development but not essential for the survival or differentiation of mature T cells. *Mol. Cell. Biol.* **32**, 1984-1997.
Goodrich, J. A. and Tjian, R. (2010). Unexpected roles for core promoter recognition factors in cell-type-specific transcription and gene regulation. *Nat. Rev. Genet.* **11**, 549-558.
Goulding, M. D., Chalepakis, G., Deutsch, U., Erselius, J. R. and Gruss, P. (1991). Pax-3, a novel murine DNA binding protein expressed during early neurogenesis. *EMBO J.* **10**, 1135-1147.
Gouti, M., Tsakiridis, A., Wymeersch, F. J., Huang, Y., Kleinjung, J., Wilson, V. and Briscoe, J. (2014). In vitro generation of neuromesodermal progenitors reveals distinct roles for Wnt signalling in the specification of spinal cord and paraxial mesoderm identity. *PLoS Biol.* **12**, e1001937.
Hubaud, A. and Pourquié, O. (2014). Signalling dynamics in vertebrate segmentation. *Nat. Rev. Mol. Cell Biol.* **15**, 709-721.
Indra, A. K., Mohan, W. S., Frontini, M., Scheer, E., Messaddeq, N., Metzger, D. and Tora, L. (2005). TAF10 is required for the establishment of skin barrier function in foetal, but not in adult mouse epidermis. *Dev. Biol.* **285**, 28-37.
Jacq, X., Brou, C., Lutz, Y., Davidson, I., Chambon, P. and Tora, L. (1994). Human TAFII30 is present in a distinct TFIID complex and is required for transcriptional activation by the estrogen receptor. *Cell* **79**, 107-117.
Kirschner, D. B., vom Baur, E., Thibault, C., Sanders, S. L., Gangloff, Y.-G., Davidson, I., Weil, P. A. and Tora, L. (2002). Distinct mutations in yeast TAF(II)25 differentially affect the composition of TFIID and SAGA complexes as well as global gene expression patterns. *Mol. Cell. Biol.* **22**, 3178-3193.
Krol, A. J., Roellig, D., Dequéant, M.-L., Tassy, O., Glynn, E., Hattem, G., Mushegian, A., Oates, A. C. and Pourquié, O. (2011). Evolutionary plasticity of segmentation clock networks. *Development* **138**, 2783-2792.
Leurent, C., Sanders, S., Ruhlmann, C., Mallouh, V., Weil, P. A., Kirschner, D. B., Tora, L. and Schultz, P. (2002). Mapping histone fold TAFs within yeast TFIID. *EMBO J.* **21**, 3424-3433.
Levine, M., Cattoglio, C. and Tjian, R. (2014). Looping back to leap forward: transcription enters a new era. *Cell* **157**, 13-25.
Lin, Z., Yang, H., Kong, Q., Li, J., Lee, S.-M., Gao, B., Dong, H., Wei, J., Song, J., Zhang, D. D. et al. (2012). USP22 antagonizes p53 transcriptional activation by deubiquitinating Sirt1 to suppress cell apoptosis and is required for mouse embryonic development. *Mol. Cell* **46**, 484-494.
Liu, Y., Zhao, J., Zhang, W., Gan, J., Hu, C., Huang, G. and Zhang, Y. (2015). lncRNA GAS5 enhances G1 cell cycle arrest via binding to YBX1 to regulate p21 expression in stomach cancer. *Sci. Rep.* **5**, 10159.
Ma, C., Shi, X., Zhu, Q., Li, Q., Liu, Y., Yao, Y. and Song, Y. (2015). The growth arrest-specific transcript 5 (GAS5): a pivotal tumor suppressor long noncoding RNA in human cancers. *Tumor Biol.* **37**, 1437-1444.
Mansouri, A., Yokota, Y., Wehr, R., Copeland, N. G., Jenkins, N. A. and Gruss, P. (1997). Paired-related murine homeobox gene expressed in the developing sclerotome, kidney, and nervous system. *Dev. Dyn.* **210**, 53-65.
McGrew, M. J., Dale, J. K., Fraboulet, S. and Pourquié, O. (1998). The lunatic fringe gene is a target of the molecular clock linked to somite segmentation in avian embryos. *Curr. Biol.* **8**, 979-982.
Metzger, D., Scheer, E., Soldatov, A. and Tora, L. (1999). Mammalian TAF(II)30 is required for cell cycle progression and specific cellular differentiation programmes. *EMBO J.* **18**, 4823-4834.
Mohan, W. S., Scheer, E., Wendling, O., Metzger, D. and Tora, L. (2003). TAF10 (TAF(II)30) is necessary for TFIID stability and early embryogenesis in mice. *Mol. Cell. Biol.* **23**, 4307-4318.
Morales, A. V., Yasuda, Y. and Ish-Horowicz, D. (2002). Periodic Lunatic fringe expression is controlled during segmentation by a cyclic transcriptional enhancer responsive to notch signaling. *Dev. Cell* **3**, 63-74.
Müller, F., Zaucker, A. and Tora, L. (2010). Developmental regulation of transcription initiation: more than just changing the actors. *Curr. Opin. Genet. Dev.* **20**, 533-540.
Nagy, A., Gertsenstein, M., Vintersten, K. and Behringer, R. R. (2002). *Manipulating the Mouse Embryo*, 3rd edn. Cold Spring Harbor: Cold Spring Harbor Laboratory Press.
Neidhardt, L. M., Kispert, A. and Herrmann, B. G. (1997). A mouse gene of the paired-related homeobox class expressed in the caudal somite compartment and in the developing vertebral column, kidney and nervous system. *Dev. Genes Evol.* **207**, 330-339.
Niederreither, K., McCaffery, P., Dräger, U. C., Chambon, P. and Dollé, P. (1997). Restricted expression and retinoic acid-induced downregulation of the retinaldehyde dehydrogenase type 2 (RALDH-2) gene during mouse development. *Mech. Dev.* **62**, 67-78.
Niwa, Y., Masamizu, Y., Liu, T., Nakayama, R., Deng, C.-X. and Kageyama, R. (2007). The initiation and propagation of Hes7 oscillation are cooperatively regulated by Fgf and notch signaling in the somite segmentation clock. *Dev. Cell* **13**, 298-304.
Ott, M. O., Bober, E., Lyons, G., Arnold, H. and Buckingham, M. (1991). Early expression of the myogenic regulatory gene, myf-5, in precursor cells of skeletal muscle in the mouse. *Development* **111**, 1097-1107.

DEVELOPMENT

Papadopoulos, P., Gutiérrez, L., Demmers, J., Scheer, E., Pourfarzad, F., Papageorgiou, D. N., Karkoulia, E., Strouboulis, J., van de Werken, H. J. G., van der Linden, R. et al. (2015). TAF10 interacts with the GATA1 transcription factor and controls mouse erythropoiesis. *Mol. Cell. Biol.* **35**, 2103-2118.

Perantoni, A. O. (2005). Inactivation of FGF8 in early mesoderm reveals an essential role in kidney development. *Development* **132**, 3859-3871.

Pickard, M. and Williams, G. (2015). Molecular and cellular mechanisms of action of tumour suppressor GAS5 lncRNA. *Genes* **6**, 484-499.

Pourquié, O. (2011). Vertebrate segmentation: from cyclic gene networks to scoliosis. *Cell* **145**, 650-663.

Rocancourt, D., Bonnerot, C., Jouin, H., Emerman, M. and Nicolas, J. F. (1990). Activation of a beta-galactosidase recombinant provirus: application to titration of human immunodeficiency virus (HIV) and HIV-infected cells. *J. Virol.* **64**, 2660-2668.

Saga, Y., Hata, N., Koseki, H. and Taketo, M. M. (1997). Mesp2: a novel mouse gene expressed in the presegmented mesoderm and essential for segmentation initiation. *Genes Dev.* **11**, 1827-1839.

Sainsbury, S., Bernecky, C. and Cramer, P. (2015). Structural basis of transcription initiation by RNA polymerase II. *Nat. Rev. Mol. Cell Biol.* **16**, 129-143.

Sapountzi, V. and Côté, J. (2011). MYST-family histone acetyltransferases: beyond chromatin. *Cell. Mol. Life Sci.* **68**, 1147-1156.

Soriano, P. (1999). Generalized lacZ expression with the ROSA26 Cre reporter strain. *Nat. Genet.* **21**, 70-71.

Soutoglou, E., Demény, M. A., Scheer, E., Fienga, G., Sassone-Corsi, P. and Tora, L. (2005). The nuclear import of TAF10 is regulated by one of its three histone fold domain-containing interaction partners. *Mol. Cell. Biol.* **25**, 4092-4104.

Spedale, G., Timmers, H. T. M. and Pijnappel, W. W. M. P. (2012). ATAC-king the complexity of SAGA during evolution. *Genes Dev.* **26**, 527-541.

Srivastava, D., Thomas, T., Lin, Q., Kirby, M. L., Brown, D. and Olson, E. N. (1997). Regulation of cardiac mesodermal and neural crest development by the bHLH transcription factor, dHAND. *Nat. Genet.* **16**, 154-160.

Tatarakis, A., Margaritis, T., Martinez-Jimenez, C. P., Kouskouti, A., Mohan, W. S., Haroniti, A., Kafetzopoulos, D., Tora, L. and Talianidis, I. (2008). Dominant and redundant functions of TFIID involved in the regulation of hepatic genes. *Mol. Cell* **31**, 531-543.

Timmers, H. T. and Sharp, P. A. (1991). The mammalian TFIID protein is present in two functionally distinct complexes. *Genes Dev.* **5**, 1946-1956.

Trowitzsch, S., Viola, C., Scheer, E., Conic, S., Chavant, V., Fournier, M., Papai, G., Ebong, I.-O., Schaffitzel, C., Zou, J. et al. (2015). Cytoplasmic TAF2-TAF8-TAF10 complex provides evidence for nuclear holo-TFIID assembly from preformed submodules. *Nat. Commun.* **6**, 6011.

Tzouanacou, E., Wegener, A., Wymeersch, F. J., Wilson, V. and Nicolas, J.-F. (2009). Redefining the progression of lineage segregations during mammalian embryogenesis by clonal analysis. *Dev. Cell* **17**, 365-376.

Vannini, A. and Cramer, P. (2012). Conservation between the RNA polymerase I, II, and III transcription initiation machineries. *Mol. Cell* **45**, 439-446.

Ventura, A., Kirsch, D. G., McLaughlin, M. E., Tuveson, D. A., Grimm, J., Lintault, L., Newman, J., Reczek, E. E., Weissleder, R. and Jacks, T. (2007). Restoration of p53 function leads to tumour regression in vivo. *Nature* **445**, 661-665.

Vincent, S. D., Dunn, N. R., Sciammas, R., Shapiro-Shalef, M., Davis, M. M., Calame, K., Bikoff, E. K. and Robertson, E. J. (2005). The zinc finger transcriptional repressor Blimp1/Prdm1 is dispensable for early axis formation but is required for specification of primordial germ cells in the mouse. *Development* **132**, 1315-1325.

Vincent, S. D., Mayeuf-Louchart, A., Watanabe, Y., Brzezinski, J. A., Miyagawa-Tomita, S., Kelly, R. G. and Buckingham, M. (2014). Prdm1 functions in the mesoderm of the second heart field, where it interacts genetically with Tbx1, during outflow tract morphogenesis in the mouse embryo. *Hum. Mol. Genet.* **23**, 5087-5101.

Voss, A. K., Thomas, T., Petrou, P., Anastassiadis, K., Schöler, H. and Gruss, P. (2000). Taube nuss is a novel gene essential for the survival of pluripotent cells of early mouse embryos. *Development* **127**, 5449-5461.

Wang, L. and Dent, S. Y. R. (2014). Functions of SAGA in development and disease. *Epigenomics* **6**, 329-339.

Weake, V. M., Dyer, J. O., Seidel, C., Box, A., Swanson, S. K., Peak, A., Florens, L., Washburn, M. P., Abmayr, S. M. and Workman, J. L. (2011). Post-transcription initiation function of the ubiquitous SAGA complex in tissue-specific gene activation. *Genes Dev.* **25**, 1499-1509.

Wittler, L., Shin, E.-H., Grote, P., Kispert, A., Beckers, A., Gossler, A., Werber, M. and Herrmann, B. G. (2007). Expression of Msgn1 in the presomitic mesoderm is controlled by synergism of WNT signalling and Tbx6. *EMBO Rep.* **8**, 784-789.

Xu, W., Edmondson, D. G., Evrard, Y. A., Wakamiya, M., Behringer, R. R. and Roth, S. Y. (2000). Loss of Gcn5l2 leads to increased apoptosis and mesodermal defects during mouse development. *Nat. Genet.* **26**, 229-232.

Yamauchi, T., Yamauchi, J., Kuwata, T., Tamura, T., Yamashita, T., Bae, N., Westphal, H., Ozato, K. and Nakatani, Y. (2000). Distinct but overlapping roles of histone acetylase PCAF and of the closely related PCAF-B/GCN5 in mouse embryogenesis. *Proc. Natl. Acad. Sci. USA* **97**, 11303-11306.

Yoon, J. K., Moon, R. T. and Wold, B. (2000). The bHLH class protein pMesogenin1 can specify paraxial mesoderm phenotypes. *Dev. Biol.* **222**, 376-391.

Zeller, R., López-Ríos, J. and Zuniga, A. (2009). Vertebrate limb bud development: moving towards integrative analysis of organogenesis. *Nat. Rev. Genet.* **10**, 845-858.

Zhou, H., Grubisic, I., Zheng, K., He, Y., Wang, P. J., Kaplan, T. and Tjian, R. (2013a). Taf7l cooperates with Trf2 to regulate spermiogenesis. *Proc. Natl. Acad. Sci. USA* **110**, 16886-16891.

Zhou, H., Kaplan, T., Li, Y., Grubisic, I., Zhang, Z., Wang, P. J., Eisen, M. B. and Tjian, R. (2013b). Dual functions of TAF7L in adipocyte differentiation. *Elife* **2**, e00170.

Zybailov, B., Mosley, A. L., Sardiu, M. E., Coleman, M. K., Florens, L. and Washburn, M. P. (2006). Statistical analysis of membrane proteome expression changes in Saccharomyces cerevisiae. *J. Proteome Res.* **5**, 2339-2347.

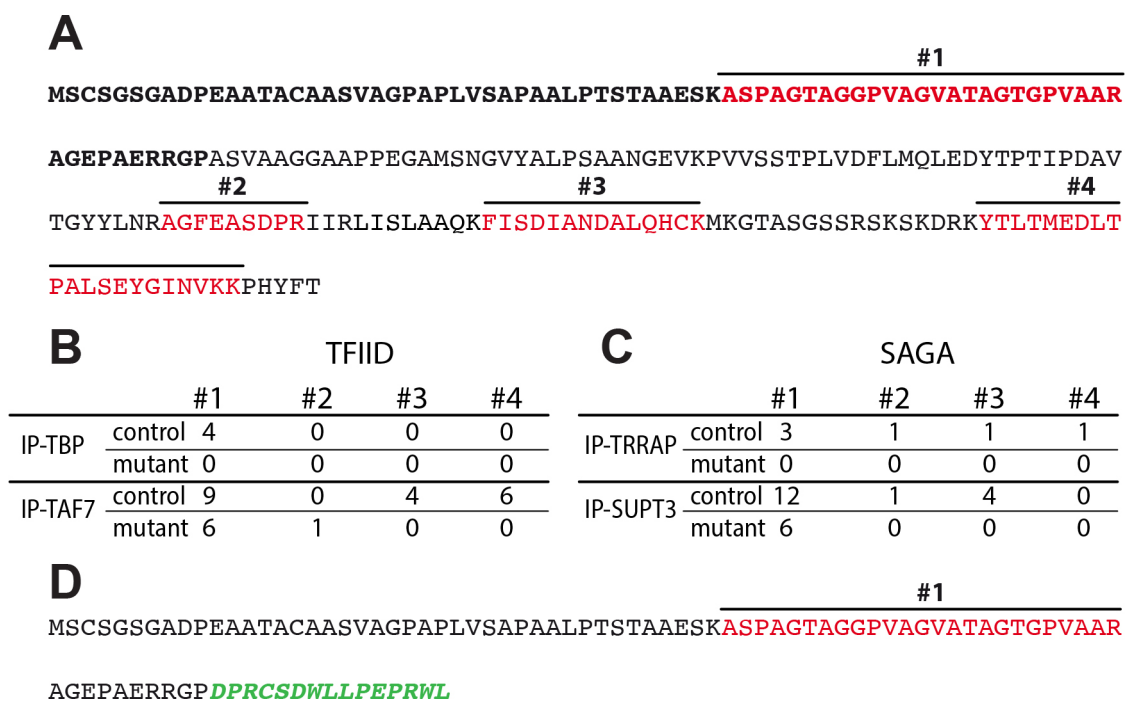DEVELOPMENT

Supplementary Figures
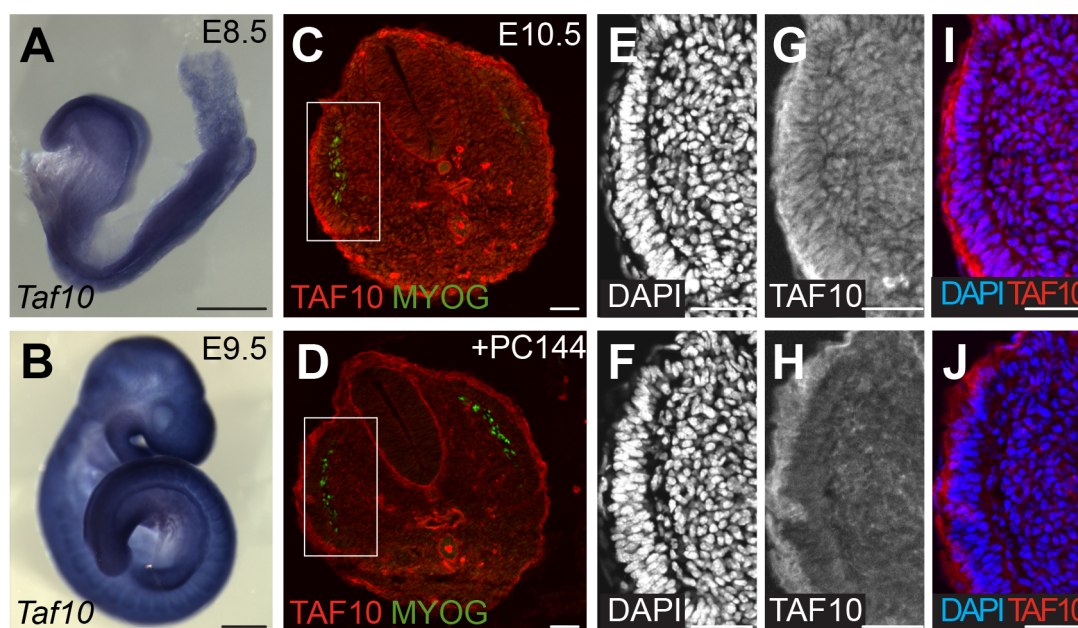
Fig. S1. TAF10 is expressed in the nuclei of the embryo. (A-B) Whole-mount *in situ* hybridization of *Taf10* at E8.5 (A) and E9.5 (B). (C-J) Co-immunolocalization of TAF10, Myogenin and DAPI in E10.5 tail transverse sections. (C-D) Colocalization of TAF10 (red) and Myogenin (MYOG, green). (E-J) DAPI (E,F), TAF10 (G,H) and merge (I,J) magnifications corresponding to the boxes indicated in C and D. (D,F,H,J) Competition with the PC144 peptide used to raise the anti-TAF10 antibody. Nuclear signal of TAF10 (D,H,J) is abolished without affecting the Myogenin signal (D). The non nuclear signal that persists after peptide competition is not specific. Scale bars in A-B and C-J represent 500 μm and 50 μm, respectively.
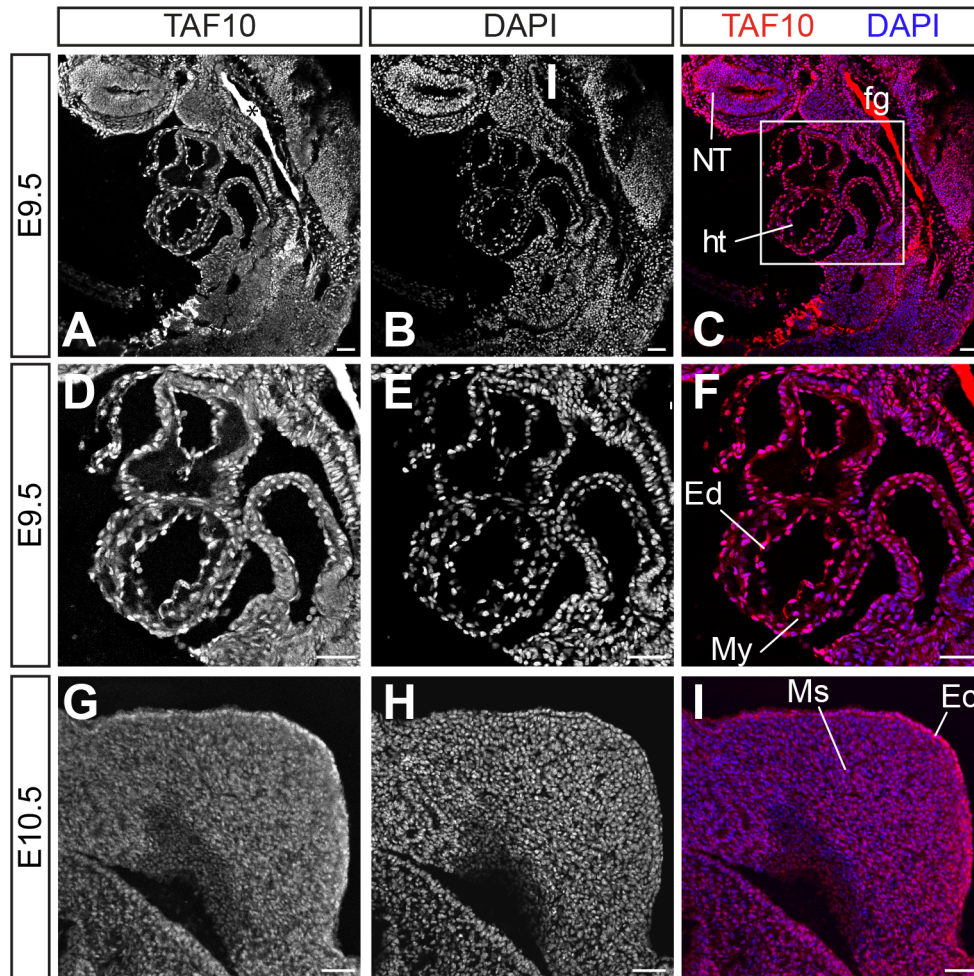
Fig. S2. TAF10 is ubiquitously expressed in the embryo. (A-I) Immunolocalization of TAF10 (A,D,G) and DAPI (B,E,H) on wild type embryo sections at E9.5 (A-F) and E10.5 (G-I). (A-C) Sagittal section at the level of the anterior part of the embryo. The asterisk marks the trapping of the secondary antibody in the foregut pocket. (D-F) is a magnification of the region indicated in C, focusing on the heart. (G-I) is a section at the level of the limb bud. NT; neural tube, ht; heart, fg; foregut; Ed; endocardium, My; myocardium, Ms; mesenchyme, Ec; ectoderm. Scale bars represent 50 μm.
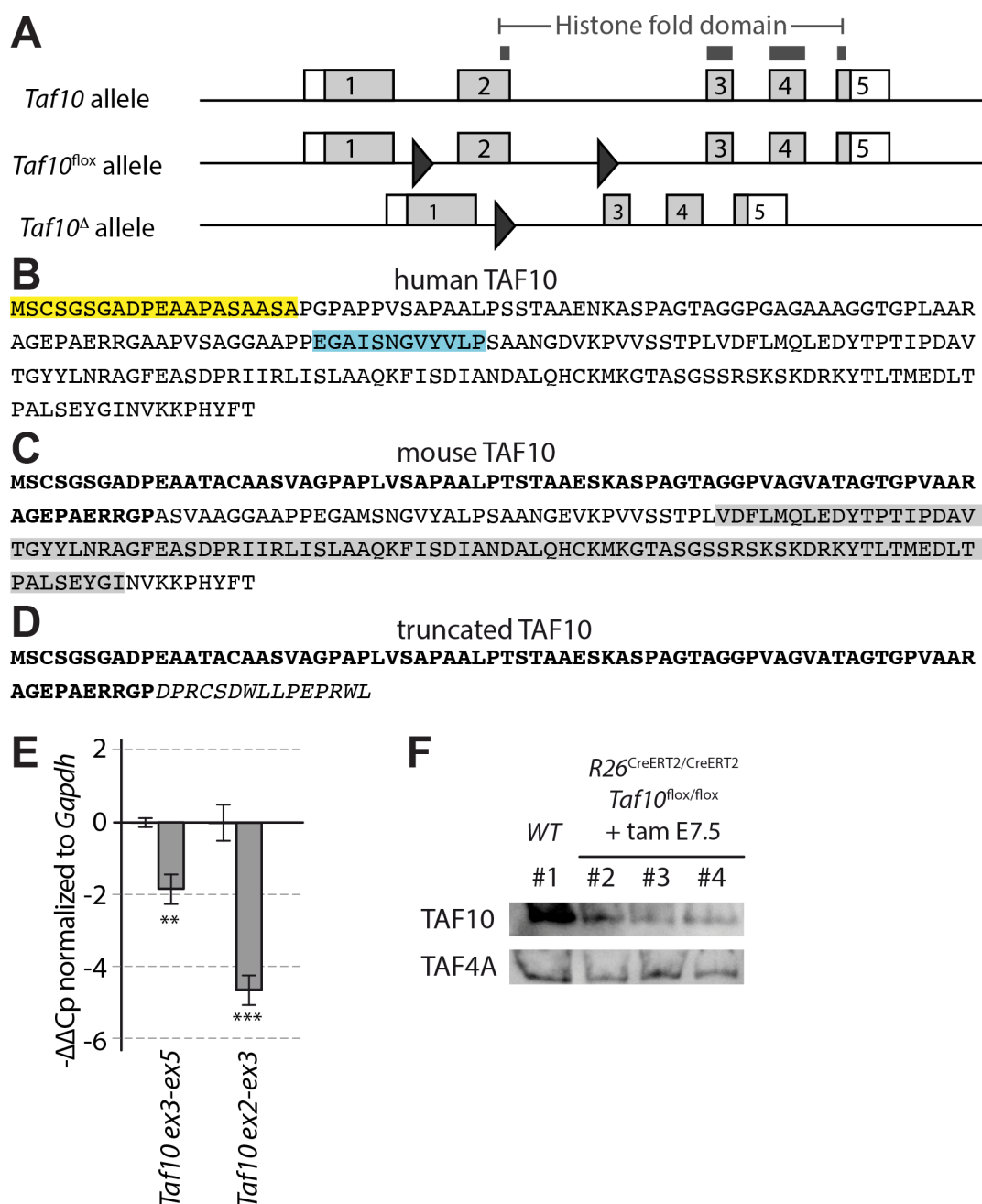
Fig. S3. Deletion of *Taf10*. (A) Strategy of the generation of the *Taf10* deletion using the *Taf10*^flox allele (Mohan et al., 2003). The exon 2 is deleted upon Cre expression. The coding sequences of the Histone Fold Domain (HFD) is highlighted by dark grey bars. The deleted allele can theoretically produce a truncated protein that does not contain the HFD, coded by exon 1 and but exon 3 that is out of frame. (B) Protein sequence of the human TAF10: the sequence of the peptides used to raise the 23TA1H8 (yellow) and 6TA2B11 (blue) anti-TAF10 antibodies (C,D) Protein sequence of the murine wild type TAF10 (C) and of the truncated protein (D) potentially present after deletion. Coding sequences of exon 1 are indicated in bold characters. The new extra 15 amino-acids encoded by exon 3 are indicated in italics. The HFD is highlighted in grey. (E) RT-qPCR analysis from tail tips of E9.25 control (white) and *TCre*/+;*Taf10*^flox/flox mutant (grey) tail tips. *Taf10 ex3-ex5* amplifies a sequence that is shared by the wild type and the deleted transcripts whereas *Taf10 ex2-ex3* amplifies a sequence only present in wild type transcript. -ΔΔCp are normalized to *Gapdh*. **; p-value <0.01, ***; p-value <0.001 (n=4 for *Taf10 ex2-ex3* and n=2 for *Taf10 ex3-ex5*, Aspin Welch corrected Student's t-test). The error bars indicate s.e.m. (F) Anti-TAF10 and anti-TAF4 western blot analysis of whole cell extract from E8.5 *R26*^CreERT2/CreERT2;*Taf10*^flox/flox embryos, induced at E7.5 by tamoxifen injection at E7.5.

A

#1

MSCSGSGADPEAATACAASVAGPAPLVSAPAALPTSTAAESKASPAGTAGGPVAGVATAGTGPVAAR

AGEPAERRGPASVAAGGAAPPEGAMSNGVYALPSAANGEVKPVVSSTPLVDFLMQLEDYTPTIPDAV

#2　　　　　　　　　　　#3　　　　　　　　　　　#4

TGYYLNRAGFEASDPRIIRLISLAAQKFISDIANDALQHCKMKGTASGSSRSKSKDRKYTLTMEDLT

PALSEYGINVKKPHYFT

B

TFIID

IP		#1	#2	#3	#4
IP-TBP	control	4	0	0	0
	mutant	0	0	0	0
IP-TAF7	control	9	0	4	6
	mutant	6	1	0	0

C

SAGA

IP		#1	#2	#3	#4
IP-TRRAP	control	3	1	1	1
	mutant	0	0	0	0
IP-SUPT3	control	12	1	4	0
	mutant	6	0	0	0

D

#1

MSCSGSGADPEAATACAASVAGPAPLVSAPAALPTSTAAESKASPAGTAGGPVAGVATAGTGPVAAR

AGEPAERRGP*DPRCSDWLLPEPRWL*

Fig. S4. Abnormal distribution of the TAF10 MS peptides detected in *R26Cre;Taf10* mutant embryos. (A) Localization of the MS peptides (#1 to #4) on the sequence of the full-length TAF10 protein. The peptides are indicated in red letters. The coding sequence corresponding to the first exon is highlighted in bold. (B-C) Number of TAF10 detected MS peptides in control and *R26Cre;Taf10* mutant embryos in each TFIID (B) and SAGA (C) IPs. (D) Localization of the MS peptide #1 (red) on the sequence of putative TAF10 truncated protein. The 15 extra amino-acids coded by exon 3 (not in frame) are indicated in green italics.
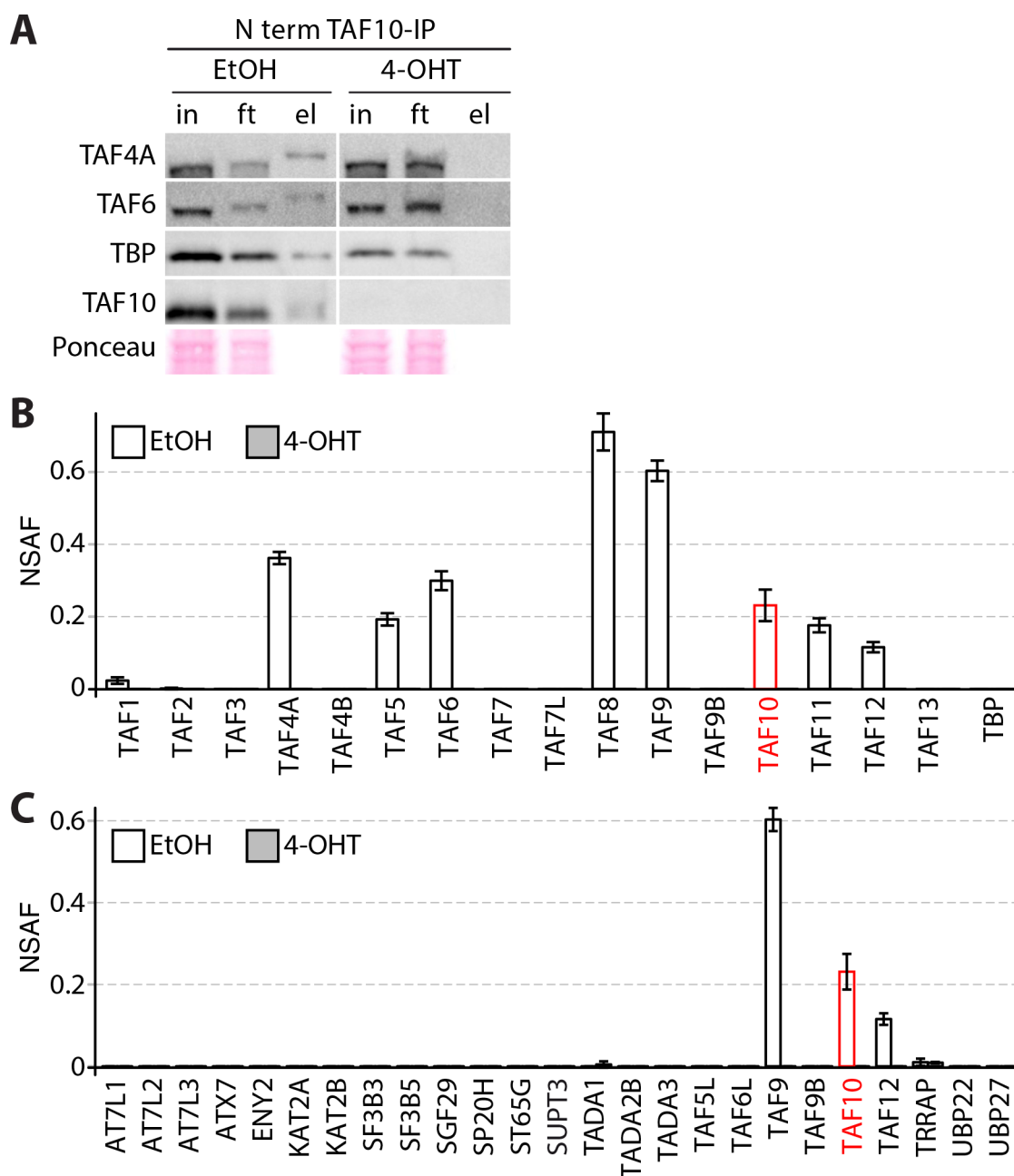
Fig. S5. The potential truncated TAF10 peptide is not able to form a TFIID complex in *Taf10* mutant ES cells (A) Western blot analysis of TBP, TAF4A, TAF6, TBP and full length TAF10 protein of input (in), flowthrough (ft) and elution (el) from Nterm-TAF10-IP from control (EtOH) and mutant (4-OHT) *Taf10* conditional mutant ES cells. (B,C) NSAF values for TFIID (B) and SAGA (C) complexes subunits of Nterm-TAF10-IP from control (EtOH) and Taf10 mutant (4-OHT) ES whole cell extracts. The control (EtOH) and mutant (4OHT) conditions are indicated in white and grey, respectively. 4-OHT; 4-hydroxy-tamoxifen.
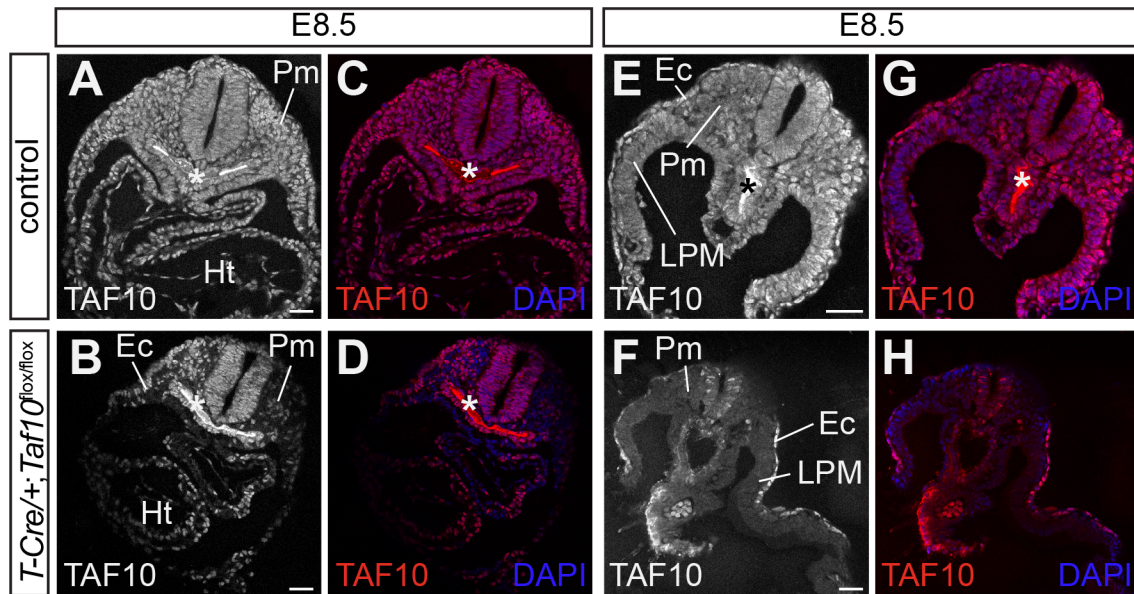
Fig. S6. TAF10 depletion is already effective in the LPM and in the paraxial mesoderm at E8.5. (A-H) TAF10 immunocolocalization on E8.5 transverse wild type (10 somites; A,C,E,G) and *T-Cre;Taf10*^{flox/flox} mutant (8 somites; B,D,F,H) embryos, at the heart (A-D) and at the posterior somites (E-H) levels. Pm; paraxial mesoderm, Ec; ectoderm, LPM; lateral plate mesoderm, Ht; heart. The asterisk (*) indicates background due to secondary antibody trapping in the endoderm. Scales bars represent 50 μm.
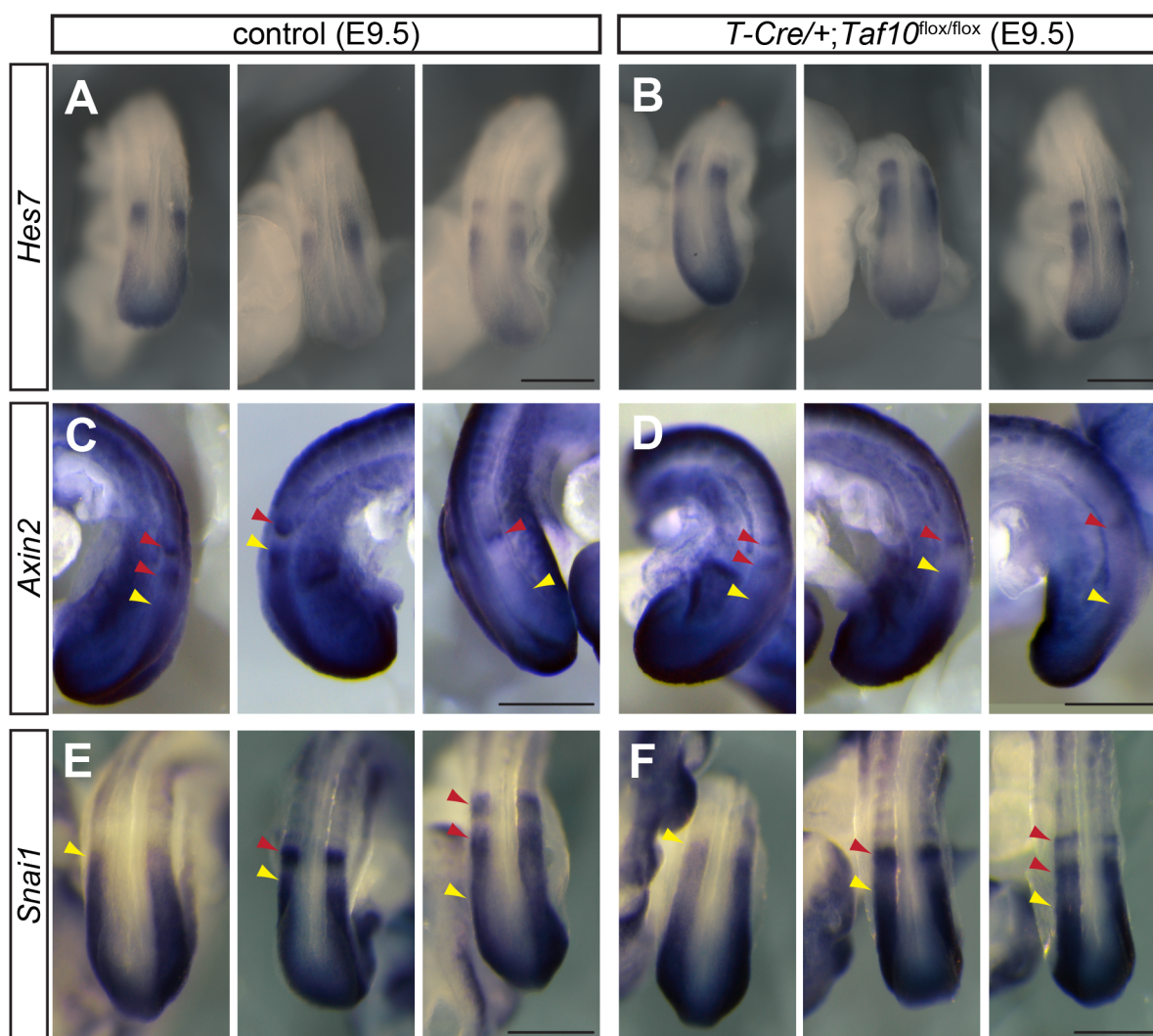
Fig. S7. Expression of the cyclic genes in the absence of TAF10. (A-F) Whole-mount *in situ* hybridization of E9.5 control (A,C,E,) and *T-Cre/+;Taf10*flox/flox mutant (B,D,F) embryos using *Hes7* (A,B), *Axin2* (C,D) and *Snai1* (E,F). For each probe, 3 different phases expression pattern are displayed, bands are highlighted by red arrows and the anterior limit of the posterior domain yellow arrows in C-F. The absence of TAF10 in the PSM does not affect the cyclic expression of Notch pathway (*Hes7*), Wnt (*Axin2*) or FGF (*Snai1*) pathways. Scale bars represent 500 μm.
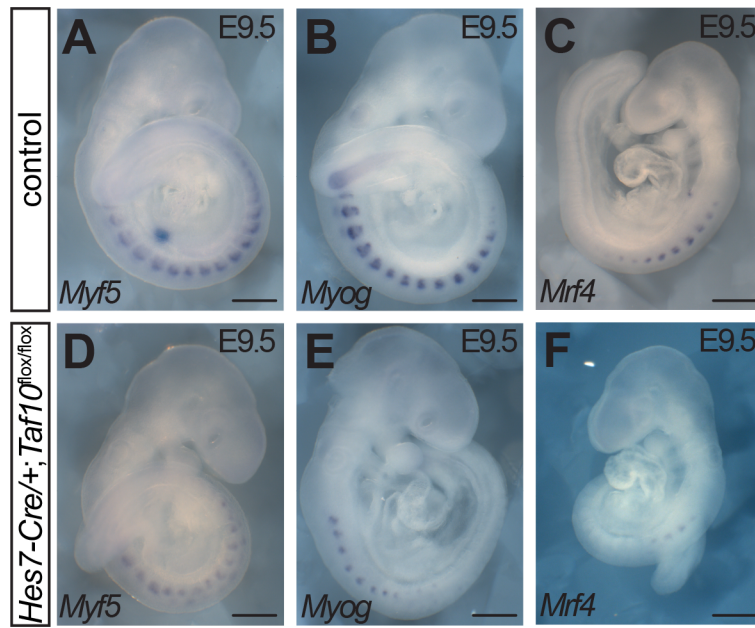
Fig. S8. Delayed myogenesis in *Hes7-Cre/+;Taf10*^{flox/flox} mutant embryos. (A-F) Whole-mount *in situ* hybridization of E9.5 control (A-C) and *Hes7-Cre/+;Taf10*^{flox/flox} mutant (D-F) embryos using *Myf5* (A,D), *Myog* (B,E) and *Mrf4* (C,F) showing decreased expression of these myogenic markers in the absence of TAF10. Scale bars represent 500 μm.
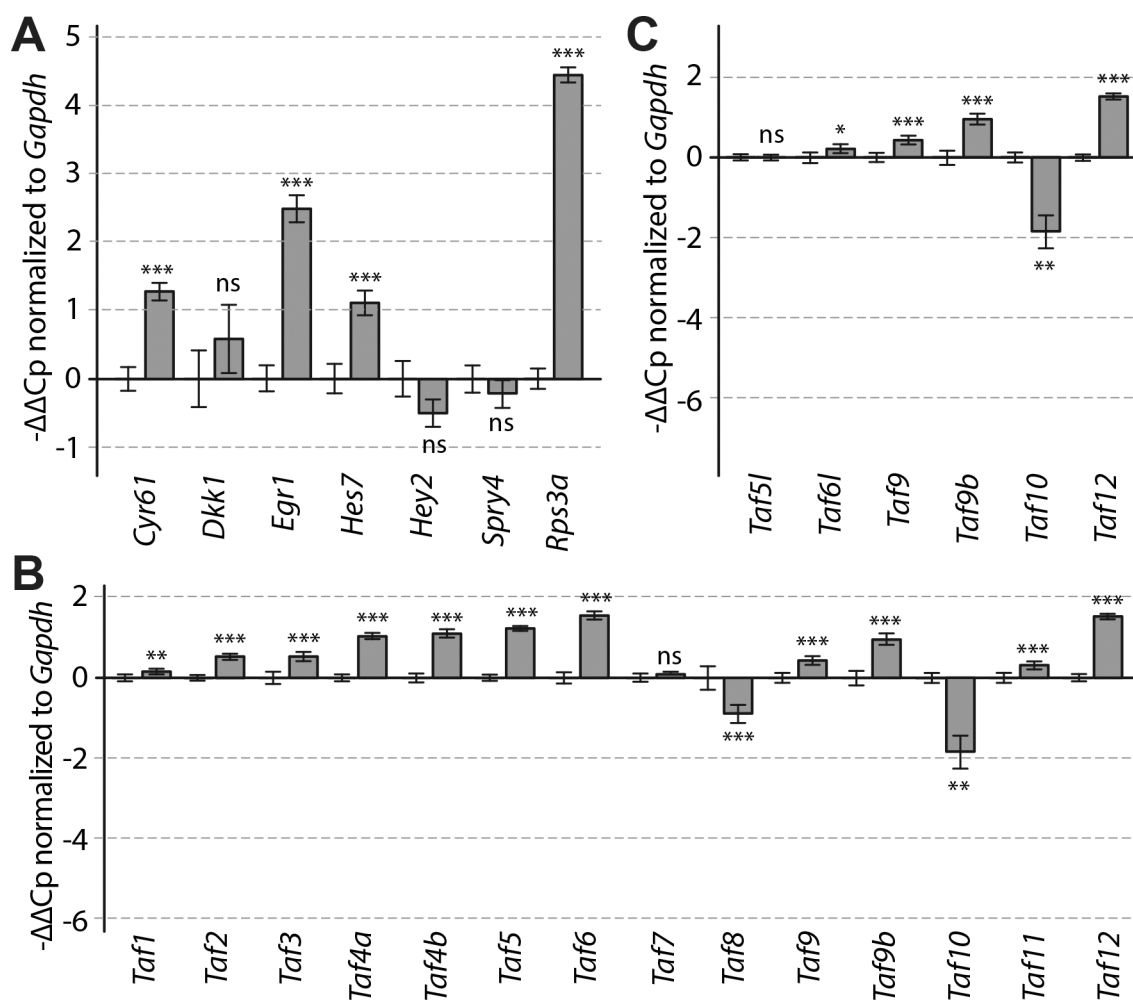
Fig. S9. Validation of the microarray analysis. (A-C) RT-qPCR analysis for cyclic genes (A), TFIID-related TAFs (B) and SAGA-related TAFs (C) from tail tips of E9.25 control (white) and *TCre/+;Taf10*flox/flox mutant (grey) tail tips. -ΔΔCp are normalized to *Gapdh*. ns; non significant, *; p-value <0.05, **; p-value <0.01, ***; p-value <0.001 (n=4 except for *Taf10* where n=2, Aspin Welch corrected Student's t-test). The error bars indicate s.e.m.

	control			
	IP TBP	*IP TAF7*	*IP SUPT3*	*IP TRRAP*
PSM* bait	10/6/7	40/37/33	19/18/20	62/65/71
SAF bait	0.02421859	0.107611082	0.046817713	0.025712615
total SAF	3.235144528	4.882771593	3.73445435	7.255567912
total protein detected	1185	1401	1213	1670

	mutant			
	IP TBP	*IP TAF7*	*IP SUPT3*	*IP TRRAP*
PSM* bait	7/7/6	32/24/29	8/15/9	67/67/52
SAF bait	0.021105319	0.082964463	0.026096693	0.02418102
total SAF	7.205885749	3.567467454	4.777603295	8.991233196
total protein detected	1525	1137	1054	1613

Table S1. Mass spectrometry results for the different IPs.
PSM*; peptide spectrum match, SAF; spectral abundance factor

Table S2. Differentially expressed genes in PSM of E9.5 *T-Cre;Taf10* mutant versus control embryos

Click here to Download Table S2

antibody	type	reference
anti-H3	rabbit polyclonal	Abcam 1791
anti-TAF10	mouse monoclonal	6TA2B11 (Mohan et al., 2003)
antiNterm-TAF10	mouse monoclonal	23TA1H8 (Wieczorek et al., 1998)
anti-TBP	mouse monoclonal	3TF13G3 (Brou et al., 1993)
anti-TAF4	mouse monoclonal	32TA2B9 (Perletti et al., 2001)
anti-TAF5	mouse monoclonal	1TA1C2 (Jacq et al., 1994)
anti-TAF6	mouse monoclonal	22TA2A1 (Wieczorek et al., 1998)
anti-TRRAP	mouse monoclonal	2TRA1B3 (Nagy et al., 2010)
anti-GST	mouse monoclonal	15TF21D10 (Nagy et al., 2010)
anti-Myogenin	rabbit polyclonal	SC-576 Santa Cruz
anti-Rabbit IgG, Alexa Fluor® 488 conjugate	goat polyclonal	Molecular Probes A-11008
anti-Mouse IgG Alexa Fluor® 546 conjugate	goat polyclonal	Molecular Probes A-11018
anti-Rabbit IgG Peroxydase conjugate	goat polyclonal	Jackson ImmunoResearch 111-035-144
anti-Mouse IgG Peroxydase conjugate	goat polyclonal	Jackson ImmunoResearch 111-036-071

Table S3. List of antibodies.

Table S4. Primer sequences.

Click here to Download Table S4

Supplementary Material and Methods

Mouse lines

Tg(*T-Cre*) (Perantoni, 2005), Tg(*Hes7-Cre*) (Niwa et al., 2007), Tg(*Luvelu*) (Aulehla et al., 2008), $R26^{CreERT2}$ (Ventura et al., 2007), $R26^{R}$ (Soriano, 1999) and $Taf10^{flox}$ (Mohan et al., 2003) lines have already been described.

Generation of antibodies

The rabbit polyclonal anti-SUPT3 (3118), anti-TAF7 (3475) and anti-TAF8 (3478) have been generated at the IGBMC antibody facility, with purified proteins. The first 285 amino-acids of human SUPT3 fused to a His tag were produced in BL21DE3 bacteria and purified with Ni-NTA beads (Qiagen). Whole protein cDNAs for human TAF7 and mouse TAF8 were produced via baculovirus in SF9 cells. For TAF8, infected SF9 cell pellet was boiled and resolved on a 10% SDS PAGE gel, then the TAF8 corresponding band was cut, frozen in liquid nitrogen and crushed. Resulting powder was directly injected into rabbits. For SUPT3 and TAF7, the purified proteins were injected into rabbits directly. The resulting sera were then purified using Affigel (Biorad) coupling followed by Poly-Prep columns (Biorad) purification against the TAF7 protein, the first 285 amino-acids SUPT3 or TAF8-TAF10 coupled protein to purify anti-TAF7, anti-SUPT3 and anti-TAF8 antibodies, respectively.

Immunoprecipitations from $R26^{CreERT2/R}$;$Taf10^{flox/flox}$ embryos

Pooled lysates from control and mutant embryos, respectively, were split in 4. IPs were performed in two series: first, anti-GST, anti-TBP, anti-TAF7 and anti-TRRAP (IP mock, IP TBP #1, IP TAF7 #1 and IP TRRAP #1). For the second series, flow through (FT) was collected after an overnight incubation, and used as inputs for the second IPs of the other complexes with fresh Dynabeads coated with fresh antibodies overnight at 4°C (IP TAF7 #2 from FT GST #1, IP TBP #2 from FT TRRAP #1, IP SUPT3 #2 from FT TBP #1 and IP TRRAP #2 from FT TAF7 #1). IP

SUPT3 #2, IP TRRAP #1, IP TAF7 #2 and IP TBP #1 that yielded the highest number of peptides for the bait were conserved for the study.

Immunoprecipitations from $R26^{CreERT2/R}$;*Taf10*$^{flox/flox}$ mouse ES cells

$R26^{CreERT2/R}$;*Taf10*$^{flox/flox}$ mouse ES cells (mES) were derived from $R26^{CreERT2/R}$;*Taf10*$^{flox/flox}$ E3.5 blastocysts (Vincent SD, unpublished data), maintained on gelatin 0.1% in PBS-coated (PAN BIOTECH) feeder-free culture plates at 37 °C in 5% CO2, in a maintenance medium composed of DMEM supplemented with 15% fetal bovine serum (FBS, Millipore), penicillin, streptomycin, 2 mM L-glutamine, 0.1 mM non essential amino acids, 0.1% β- mercaptoethanol, 1,500 U/mL LIF and 2i inhibitors (Ying et al., 2008) (CHIR99021 3μM and PD0325901 1μM (Axon medchem)). Mouse ES cells were treated with 0.01% EtOH (control) or 100nM 4-OHT (SIGMA) (mutant) for 4 days.

After 2 PBS washes at 4°C, the cells were then scrapped, collected after 20817 rcf centrifugation for 15 min at 4°C and lysed in 10% glycerol, 20 mM Hepes (pH7), 0.35 M NaCl, 1.5 mM MgCl2, 0.2 mM EDTA, 0.1% Triton X-100 with protease inhibitor cocktail (PIC, Roche) on ice. Lysates were treated 3 times with pestle stroke followed by 3 liquid nitrogen freezing-thaw cycles. Lysates were centrifuged at 20817 rcf for 15 min at 4°C and the supernatants were used directly for IPs or stored at -80°C for western blots.

Four mg inputs were incubated with Protein G Sepharose beads (SIGMA) coated with the anti N terminal TAF10 (23TA1H8) mouse monoclonal antibody (Wieczorek et al., 1998) overnight at 4°C. Immunoprecipitated proteins were washed twice 5 min with 500 mM KCl buffer (25 mM Tris-HCl HCl (pH7), 5 mM MgCl2, 10% glycerol, 0.1% NP40, 2 mM DTT, 100 mM KCl and PIC (Roche)) and eluted with 0.1 M glycine (pH2.8) for 5 min three times. Elution fractions were neutralized with 1.5 M Tris-HCl (pH8.8).

Mass spectrometry analyses and NSAF calculations

Samples were TCA precipitated, reduced, alkylated and digested with LysC and Trypsin at 37°C overnight. After C18 desalting, samples were analyzed using an Ultimate 3000 nano-RSLC (Thermo Scientific, San Jose, California) coupled in line with an linear trap Quadrupole (LTQ)-Orbitrap ELITE mass spectrometer via a nano-electrospray ionization source (Thermo Scientific). Peptide mixtures were loaded on a C18 Acclaim PepMap100 trap column (75 μm inner diameter × 2 cm, 3 μm, 100 Å; Thermo Fisher Scientific) for 3.5 min at 5 μl/min with 2% acetonitrile (ACN), 0.1% formic acid in H_2O and then separated on a C18 Accucore nano-column (75 μm inner diameter × 50 cm, 2.6 μm, 150 Å; Thermo Fisher Scientific) with a 240-min linear gradient from 5% to 50% buffer B (A: 0.1% FA in H_2O; B: 80% ACN, 0.08% FA in H_2O) followed with 10 min at 99% B. The total duration was set to 280 min at a flow rate of 200 nL/min. Peptides were analyzed by high resolution full MS scan (R240K, from 300 to 1650 m/z range) followed by 20 MS/MS events using data-dependent CID (collision induced dissociation) acquisition.

Proteins were identified by database searching using SequestHT (Thermo Fisher Scientific) with Proteome Discoverer 1.4 software (Thermo Fisher Scientific) a combined Mus musculus database (Swissprot, release 2015_11, 16730 entries) where 5 sequences of protein of interest (TrEMBL entries) were added. Precursor and fragment mass tolerances were set at 7 ppm and 0.5 Da respectively, and up to 2 missed cleavages were allowed. Oxidation (M) was set as variable modification, and carbamidomethylation (C) as fixed modification. Peptides were filtered with a false discovery rate (FDR) and rank 1: FDR at 5 %, rank 1 and proteins were identified with 1 unique peptide.

Normalized spectral abundance factor (NSAF) (Zybailov et al., 2006) normalized to the bait ($NSAF_{bait}$) were obtained as followed (PSM*; peptide spectrum match, SAF; spectral abundance factor, x; protein of interest):

$$SAF_{(x)} = \frac{PSM^*_{x(IP)} - PSM^*_{x(IPmock)}}{length(x)}$$

$$NSAF_{(x)} = \frac{SAF_{(x)}}{\sum\limits_{i=1}^{n} SAF_{(xi)}} \times 100$$

$$NSAF_{bait(x)} = \frac{NSAF_{(x)}}{NSAF_{(bait)}}$$

For the Nterm-TAF10 IP analyses, only the NSAF was calculated since the bait was not detected in the mutant conditions.

Microarrays and statistical analysis

Total RNA was prepared from 3 replicates (control and mutant), following the recommendations of the manufacturer. Biotinylated single strand cDNA targets were prepared, starting from 150 ng of total RNA, using the Ambion WT Expression Kit (Cat # 4411974) and the Affymetrix GeneChip® WT Terminal Labeling Kit (Cat # 900671) according to Affymetrix recommendations. Following fragmentation and end-labeling, 1.9 µg of cDNAs were hybridized for 16 hours at 45ºC on GeneChip® Mouse Gene 1.0 ST arrays (Affymetrix). The chips were washed and stained in the GeneChip® Fluidics Station 450 (Affymetrix) and scanned with the GeneChip® Scanner 3000 7G (Affymetrix) at a resolution of 0,7 μm. Raw data (.CEL Intensity files) were extracted from the scanned images using the Affymetrix GeneChip® Command Console (AGCC) version 3.2.

Background correction, quantile normalization and summarization by median polish were performed using RMA (Bioconductor package version 2.14 (R version 3.1.0)). Data were filtered automatically by estimating the 100th lowest value of the data series and setting up a background threshold to 3 times this value and by removing manually all the pseudogenes and the expressed sequences. After filtration, 18064 out of 34760 probesets (51.9%) remained. Statistical analysis was performed using the FCROS package version 1.1 (R version 3.1.0) (Dembélé and Kastner,

2014) that calculates a f value. Differences are considered significant for f value below 0.025 or above 0.0975. Scatter plot and vulcano plots were performed using R software version 3.1.0.

RT-qPCR and statistical analyses

Unless specified, primers (Table S4) were designed using Primer3 (www.ncbi.nlm.nih.gov/tools/primer-blast) and validated.

To compare RNA polymerases I and II transcriptions, each Cp values were normalised by dividing each Cp to the mean of all Cp (mutants and controls) for one set of primers. Data were analysed using a Student's *t*-test with an Aspin Welch correction.

For the gene expression analyses from tail tips, -ΔΔCp values were calculated first by normalizing each Cp to the mean of the Cps for *Gapdh*, then by subtracting each ΔCp of the different controls from the ΔCp of the sample of interest for a given gene of interest, therefore generating 2x16 -ΔΔCp values for mutants and controls, for one given gene. Data were analysed using a Student's *t*-test with an Aspin Welch correction. Calculations and graphs were obtained using R (3.1.0).

References

Aulehla, A., Wiegraebe, W., Baubet, V., Wahl, M. B., Deng, C., Taketo, M., Lewandoski, M. and Pourquié, O. (2008). A beta-catenin gradient links the clock and wavefront systems in mouse embryo segmentation. *Nat Cell Biol* **10**, 186–193.

Brou, C., Chaudhary, S., Davidson, I., Lutz, Y., Wu, J., Egly, J. M., Tora, L. and Chambon, P. (1993). Distinct TFIID complexes mediate the effect of different transcriptional activators. *EMBO J* **12**, 489–499.

Dembélé, D. and Kastner, P. (2014). Fold change rank ordering statistics: a new method for detecting differentially expressed genes. *BMC Bioinformatics* **15**, 14.

Jacq, X., Brou, C., Lutz, Y., Davidson, I., Chambon, P. and Tora, L. (1994). Human TAFII30 is present in a distinct TFIID complex and is required for transcriptional activation by the estrogen receptor. *Cell* **79**, 107–117.

Mohan, W. S., Scheer, E., Wendling, O., Metzger, D. and Tora, L. (2003). TAF10 (TAF(II)30) is necessary for TFIID stability and early embryogenesis in mice. *Mol Cell Biol* **23**, 4307–4318.

Nagy, Z., Riss, A., Fujiyama, S., Krebs, A., Orpinell, M., Jansen, P., Cohen, A., Stunnenberg, H. G., Kato, S. and Tora, L. (2010). The metazoan ATAC and SAGA coactivator HAT complexes regulate different sets of inducible target genes. *Cell Mol Life Sci* **67**, 611–628.

Niwa, Y., Masamizu, Y., Liu, T., Nakayama, R., Deng, C.-X. and Kageyama, R. (2007). The initiation and propagation of Hes7 oscillation are cooperatively regulated by Fgf and notch signaling in the somite segmentation clock. *Dev Cell* **13**, 298–304.

Perantoni, A. O. (2005). Inactivation of FGF8 in early mesoderm reveals an essential role in kidney development. *Development* **132**, 3859–3871.

Perletti, L., Kopf, E., Carré, L. and Davidson, I. (2001). Coordinate regulation of RARgamma2, TBP, and TAFII135 by targeted proteolysis during retinoic acid-induced differentiation of F9 embryonal carcinoma cells. *BMC Mol. Biol.* **2**, 4.

Soriano, P. (1999). Generalized lacZ expression with the ROSA26 Cre reporter strain. *Nat Genet* **21**, 70–71.

Ventura, A., Kirsch, D. G., McLaughlin, M. E., Tuveson, D. A., Grimm, J., Lintault, L., Newman, J., Reczek, E. E., Weissleder, R. and Jacks, T. (2007). Restoration of p53 function leads to tumour regression in vivo. *Nature* **445**, 661–665.

Wieczorek, E., Brand, M., Jacq, X. and Tora, L. (1998). Function of TAF(II)-containing complex without TBP in transcription by RNA polymerase II. *Nature* **393**, 187–191.

Ying, Q.-L., Wray, J., Nichols, J., Batlle-Morera, L., Doble, B., Woodgett, J., Cohen, P. and Smith, A. (2008). The ground state of embryonic stem cell self-renewal. *Nature* **453**, 519–523.

Zybailov, B., Mosley, A. L., Sardiu, M. E., Coleman, M. K., Florens, L. and Washburn, M. P. (2006). Statistical analysis of membrane proteome expression changes in Saccharomyces cerevisiae. *J. Proteome Res.* **5**, 2339–2347.